SKIN

Copyright © 2018 The Authors, some rights reserved; exclusive licensee American Association for the Advancement of Science. No claim to original U.S. Government Works

A protective Langerhans cell–keratinocyte axis that is dysfunctional in photosensitivity

William D. Shipman[1,2,3], Susan Chyou[3], Anusha Ramanathan[3], Peter M. Izmirly[4], Sneh Sharma[5,6], Tania Pannellini[3], Dragos C. Dasoveanu[3,7], Xiaoping Qing[3], Cynthia M. Magro[8], Richard D. Granstein[9], Michelle A. Lowes[10], Eric G. Pamer[6], Daniel H. Kaplan[11,12], Jane E. Salmon[2,3,13,14], Babak J. Mehrara[15], James W. Young[5,6,10,13,16], Robert M. Clancy[4], Carl P. Blobel[7,13,17,18], Theresa T. Lu[2,3,14,19]*

Photosensitivity, or skin sensitivity to ultraviolet radiation (UVR), is a feature of lupus erythematosus and other autoimmune and dermatologic conditions, but the mechanistic underpinnings are poorly understood. We identify a Langerhans cell (LC)–keratinocyte axis that limits UVR-induced keratinocyte apoptosis and skin injury via keratinocyte epidermal growth factor receptor (EGFR) stimulation. We show that the absence of LCs in Langerin–diphtheria toxin subunit A (DTA) mice leads to photosensitivity and that, in vitro, mouse and human LCs can directly protect keratinocytes from UVR-induced apoptosis. LCs express EGFR ligands and a disintegrin and metalloprotease 17 (ADAM17), the metalloprotease that activates EGFR ligands. Deletion of ADAM17 from LCs leads to photosensitivity, and UVR induces LC ADAM17 activation and generation of soluble active EGFR ligands, suggesting that LCs protect by providing activated EGFR ligands to keratinocytes. Photosensitive systemic lupus erythematosus (SLE) models and human SLE skin show reduced epidermal EGFR phosphorylation and LC defects, and a topical EGFR ligand reduces photosensitivity. Together, our data establish a direct tissue-protective function for LCs, reveal a mechanistic basis for photosensitivity, and suggest EGFR stimulation as a treatment for photosensitivity in lupus erythematosus and potentially other autoimmune and dermatologic conditions.

INTRODUCTION

Photosensitivity, a sensitivity to ultraviolet radiation (UVR) whereby even ambient sunlight exposure can result in inflammatory skin lesions, is a common feature in cutaneous and systemic forms of lupus erythematosus and can also occur with other autoimmune conditions, a number of dermatologic conditions, and as a response to drugs such as fluoroquinolone antibiotics (*1*–*3*). The photosensitive lesions can be disfiguring and, in systemic lupus erythematosus (SLE), can be associated with systemic disease flares (*1*, *2*). The pathogenesis of photosensitivity is poorly understood, and treatments consist mainly of sun avoidance and sunscreen to prevent lesion development (*2*). A better understanding of the mechanistic basis of photosensitivity could lead to improved disease treatment.

Keratinocyte apoptosis occurs rapidly after UVR exposure, and photosensitivity is associated with increased keratinocyte apoptosis (*4*, *5*). In autoimmune diseases, apoptotic keratinocytes can display autoantigens that bind autoantibodies, leading to complement activation and sustained skin inflammation (*1*, *5*). The localization of "sunburn cells," or apoptotic keratinocytes, with lupus erythematosus skin lesions (*6*) further supports the idea that keratinocyte apoptosis is part of the pathophysiology. Keratinocytes are critical for normal skin barrier function (*7*), and even in the absence of autoimmunity, increased keratinocyte death and failure to compensate have the potential to lead to skin injury and inflammation (*8*). However, mechanisms that limit UVR-induced keratinocyte apoptosis that are dysfunctional in photosensitivity are not well understood.

In addition to keratinocytes, the epidermis contains a population of well-described Langerin$^+$ dendritic antigen-presenting cells, known as Langerhans cells (LCs). LCs are primarily associated with their antigen presentation functions: capturing antigens in the epidermis, migrating from the skin to the draining lymph node, and initiating T cell responses (*9*, *10*). In lupus skin lesions, LCs have an abnormal morphology and are reduced in number (*11*), suggesting the possibility of a regulatory role. However, in the MRL-*Fas*^{lpr} SLE mouse model, the role of LCs in spontaneous (that is, non-UVR–induced) skin lesion development has been examined with mixed conclusions; constitutive LC absence had no effect on skin lesions (*12*), whereas acute depletion of LCs and Langerin$^+$ dermal dendritic cells (DCs) increased lesions, and this was attributed to loss of T cell tolerance (*13*). Thus, the role of LCs in photosensitivity and as a potential direct modulator of keratinocyte function has not been explored.

We and others have recently shown that DCs can directly modulate stromal elements in lymph nodes, adipose tissues, and skin (*14*–*18*). Because LCs have DC characteristics (*9*, *10*), we asked whether LCs modulated keratinocyte survival and skin injury after UVR exposure.

[1]Weill Cornell/Rockefeller/Sloan-Kettering Tri-Institutional MD-PhD Program, New York, NY 10065, USA. [2]Immunology and Microbial Pathogenesis Program, Weill Cornell Graduate School of Medical Sciences, New York, NY 10065, USA. [3]Autoimmunity and Inflammation Program, Hospital for Special Surgery, New York, NY 10021, USA. [4]Department of Medicine, New York University School of Medicine, New York, NY 10016, USA. [5]Department of Medicine, Memorial Sloan Kettering Cancer Center, New York, NY 10065, USA. [6]Immunology Program, Sloan Kettering Institute, Memorial Sloan Kettering Cancer Center, New York, NY 10065, USA. [7]Department of Physiology, Biophysics and Systems Biology, Weill Cornell Medicine, New York, NY 10065, USA. [8]Department of Pathology and Laboratory Medicine, Weill Cornell Medicine, New York, NY 10065, USA. [9]Department of Dermatology, Weill Cornell Medicine, New York, NY 10065, USA. [10]Rockefeller University, New York, NY 10065, USA. [11]Department of Dermatology, University of Pittsburgh, PA 15260, USA. [12]Department of Immunology, University of Pittsburgh, PA 15260, USA. [13]Department of Medicine, Weill Cornell Medicine, New York, NY 10065, USA. [14]Division of Rheumatology and Pediatric Rheumatology, Hospital for Special Surgery, New York, NY 10021, USA. [15]Division of Plastic and Reconstructive Surgery, Department of Surgery, Memorial Sloan Kettering Cancer Center, New York, NY 10065, USA. [16]Adult Bone Marrow Transplantation Service, Memorial Sloan Kettering Cancer Center, New York, NY 10065, USA. [17]Arthritis and Tissue Degeneration Program, Hospital for Special Surgery, New York, NY 10021, USA. [18]Institute for Advanced Studies, Technical University Munich, Munich, Germany. [19]Department of Microbiology and Immunology, Weill Cornell Medicine, New York, NY 10065, USA.
*Corresponding author. Email: lut@hss.edu

Downloaded from http://stm.sciencemag.org/ by guest on August 20, 2018

Here, we delineate an LC-keratinocyte axis whereby LCs limit UVR-induced keratinocyte apoptosis and skin injury by activating epidermal growth factor receptor (EGFR). This axis is dysfunctional in photosensitive SLE mouse models, and there is also evidence of dysfunction in human SLE. Photosensitivity in one of the SLE models is reduced by EGFR ligand supplementation. Together, our results identify a tissue-protective function for LCs, provide insight into mechanisms that limit skin injury, and suggest that EGFR stimulation may be an approach for treatment of photosensitivity in lupus erythematosus and other diseases.

RESULTS

LCs limit UVR-induced keratinocyte apoptosis and skin injury

LCs are positioned within the epidermis with keratinocytes (fig. S1, A and B), suggesting that LCs have the potential to modulate UVR-induced keratinocyte apoptosis. To test this idea, we used the Langerin–diphtheria toxin subunit A (DTA) mouse model that is constitutively depleted of LCs (fig. S1C) but not of Langerin$^+$ dermal DCs (*19*). We treated wild-type (WT) and Langerin-DTA mice with UVR and examined the skin at 24 hours (Fig. 1A). In WT mice, epidermal LCs were reduced by half with UVR (fig. S1C), likely due to LC emigration (*9*, *10*). As expected, UVR induced an increase in activated caspase-3$^+$ cells in the epidermis (Fig. 1B, left). These cells were Langerin$^-$ (fig. S1D) and CD3$^-$ (fig. S1E), consistent with the idea that the apoptotic cells were keratinocytes. The lack of activated caspase-3$^+$ Langerin$^+$ cells also suggested that LCs were not ingesting apoptotic keratinocytes. Langerin-DTA mice showed increased numbers of activated caspase-3$^+$ keratinocytes relative to WT mice (Fig. 1B, right), and this occurred as early as 3 hours after UVR exposure (fig. S1F). Langerin-DTA mice had greater monocyte accumulation (Fig. 1C). This was associated with greater numbers of monocyte-derived DCs (fig. S1G), whereas CD11b$^-$ DCs, CD11b$^+$ DCs, macrophages, and neutrophils did not increase in Langerin-DTA mice (fig. S1G). Our UVR source provided both ultraviolet A and B radiation (*20*), and increased UVR-induced keratinocyte apoptosis and monocyte accumulation in Langerin-DTA

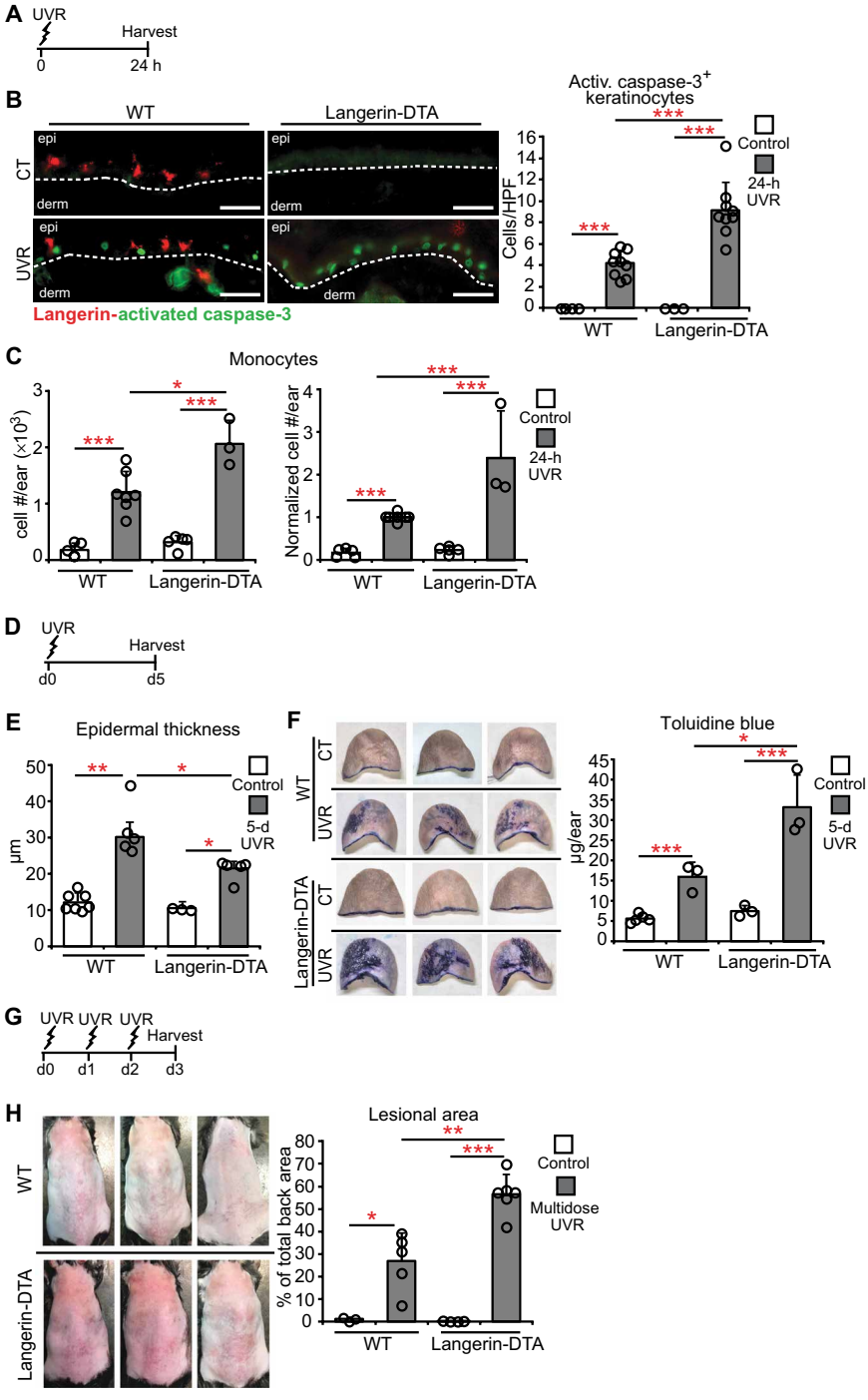

Fig. 1. LCs limit UVR-induced keratinocyte apoptosis and skin injury. (**A** to **H**) WT and Langerin-DTA mice were exposed to UVR and examined. (A) Experimental scheme for (B) and (C); ears were harvested 24 hours after UVR. (B) Activated (Activ.) caspase-3$^+$ keratinocytes per high-powered field (HPF). Left: Representative images of Langerin (red) and activated caspase-3 (green) stain. Right: Quantification ($n = 3$ to 9 mice). Scale bars, 50 μm. (C) Absolute (left) and normalized (right) monocyte numbers assessed by flow cytometry ($n = 3$ to 7 mice). (D) Experimental scheme for (E) and (F); ears were harvested 5 days (d5) after UVR. (E) Epidermal thickness ($n = 3$ to 7 mice). (F) Epidermal permeability as assessed by toluidine blue penetrance. Left: Representative images. Right: Quantification ($n = 3$ to 5 mice). (G) Experimental scheme for (H); mice were exposed to UVR for 3 days and examined 24 hours later. (H) Left: Representative images of back skin. Right: Lesional area quantification ($n = 3$ to 5 mice). Bars represent means (B, C, F, and H) or medians (E). Error bars depict SDs (B, C, F, and H) or interquartile ranges (E). *$P < 0.05$, **$P < 0.01$, ***$P < 0.001$ using two-tailed unpaired Student's t test (B, C, F, and H) or nonparametric nondirectional Mann-Whitney U test (E) after one-way analysis of variance (ANOVA). Data are from nine (B), five (C), four (E), two (F), and three (H) independent experiments.

Downloaded from http://stm.sciencemag.org/ by guest on August 20, 2018

mice remained when UVB was blocked by use of a Mylar filter (fig. S1, H to J), suggesting that LCs limit the effects of, at least, UVA. Together, these results suggested that LCs limit UVR-induced keratinocyte apoptosis and skin inflammation.

We assessed additional parameters of skin function. UVR exposure induces epidermal hyperplasia within several days (*21*), and Langerin-DTA mice showed less epidermal thickening than WT mice (Fig. 1, D and E). Epidermal barrier function is compromised despite the hyperplasia (*22*), and Langerin-DTA skin showed greater tissue penetrance of toluidine blue (*23*) than WT skin (Fig. 1F), suggesting worsened barrier function. Consistent with worsened skin function, Langerin-DTA mice showed a greater lesional area after exposure to multiple UVR doses (Fig. 1, G and H, and fig. S1K). These results together suggested that LCs limit the extent of UVR-induced skin injury.

We next attempted to assess whether the monocytes that accumulated in UVR-treated skin contributed to the UVR-induced damage. Consistent with the work of Tamoutounour *et al.* (*24*), we identified $CCR2^+$ monocytes and monocyte-derived DCs in inflamed skin, and $CD11b^+$ DCs were also $CCR2^+$ (fig. S2A). Monocytes and monocyte-derived DCs comprised the vast majority of $CCR2^+$ cells (fig. S2B). LCs were $CCR2^-$ (fig. S2C). We depleted the $CCR2^+$ cells using CCR2-DTR mice (fig. S2D) (*25*). The depletion did not alter UVR-induced keratinocyte apoptosis or epidermal thickness (fig. S2, E and F) but reduced toluidine blue penetrance (fig. S2G). Although we cannot rule out a role for the $CD11b^+$ DCs, these data raise the possibility that an increased number of infiltrating monocytes and monocyte-derived cells contributed to the worsened barrier function in Langerin-DTA mice.

LCs directly protect keratinocytes

T cells also inhabit the epidermis (Fig. 2A) (*9*), and we asked whether LCs limited UVR-induced skin injury via T cells. $Rag1^{-/-}$ Langerin-DTA mice lacking both lymphocytes and LCs showed higher UVR-induced keratinocyte apoptosis than $Rag1^{-/-}$ mice (Fig. 2B). Although $Rag1^{-/-}$ mice showed higher UVR-induced monocyte accumulation than WT mice (Fig. 2C), $Rag1^{-/-}$ Langerin-DTA mice showed even greater monocyte accumulation (Fig. 2C). These results suggested that LC-mediated skin protection was independent of antigen presentation to T cells and that LCs could potentially limit keratinocyte apoptosis directly.

We tested for direct LC-keratinocyte interactions using LC-keratinocyte cocultures. UVR induces keratinocyte apoptosis in vitro (*26*), and addition of LCs reduced the apoptosis (Fig. 2, D and E). Essentially, no activated caspase-3^+ cells were Langerin$^+$ (fig. S3A), suggesting that the LC-mediated reduction in apoptotic keratinocytes was not due to apoptotic keratinocyte ingestion and clearance. These effects were not due to phototoxicity from the phenol red–containing culture medium because results were similar in phenol red–free medium (fig. S3B). Together, these results suggested that LCs limit UVR-induced keratinocyte apoptosis and skin injury in vivo by direct interactions with keratinocytes.

LCs limit UVR-induced keratinocyte apoptosis and skin injury by stimulating epidermal EGFR

Because keratinocyte EGFR signaling protects against UVR-induced keratinocyte apoptosis (*21*, *27*) and contributes to maintaining epidermal barrier function and limiting skin inflammation (*7*, *28*), we hypothesized that the LC-mediated skin protection involved EGFR signaling. Treatment of WT mice with PD168393, an irreversible EGFR inhibitor (*29*), reduced epidermal EGFR phosphorylation at tyrosine 1068 (fig. S4, A and B), a residue associated with keratinocyte survival after UVR (*27*). Ninety-eight percent of epidermal EGFR$^+$ cells was keratinocytes (fig. S4, C and D), suggesting that the epidermal EGFR phosphorylation in Western blots reflected mainly keratinocyte

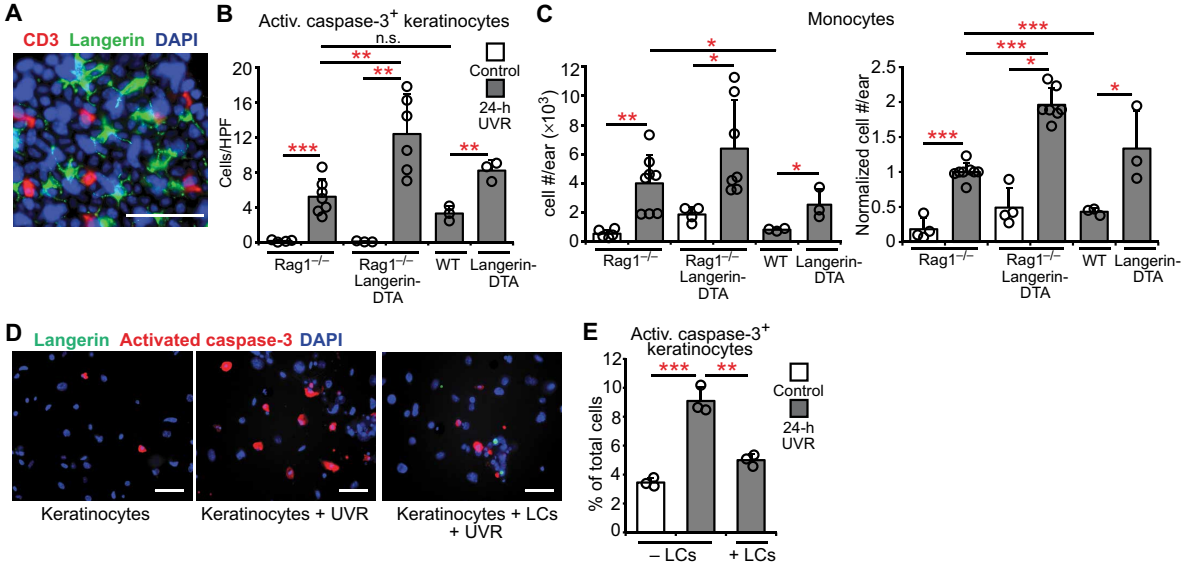

Fig. 2. LCs limit UVR-induced keratinocyte apoptosis directly. (**A**) Whole-mount stain of homeostatic mouse epidermis for CD3 (red), Langerin (green), and 4′,6-diamidino-2-phenylindole (DAPI; blue). (**B** and **C**) $Rag1^{-/-}$, $Rag1^{-/-}$ Langerin-DTA, WT, and Langerin-DTA mice were exposed to UVR, and ears were harvested 24 hours later ($n = 3$ to 8 mice). (B) Activated caspase-3^+ keratinocytes. n.s., not significant. (C) Absolute (left) and normalized (right) monocyte numbers. (**D** and **E**) Effect of LCs on keratinocyte survival in vitro. Murine keratinocyte cultures without and with LCs were exposed to UVR and examined 24 hours later ($n = 3$ mice). (D) Representative images of cultures stained for Langerin (green), activated caspase-3 (red), and DAPI (blue). (E) Activated caspase-3^+ keratinocytes. (E) Data are from five (B and C) and three (A, D, and E) independent experiments. Scale bars, 50 μm. (B, C, and E) Bars represent means. Error bars depict SDs. *$P < 0.05$, **$P < 0.01$, ***$P < 0.001$ using two-tailed unpaired Student's *t* test after one-way ANOVA.

Downloaded from http://stm.sciencemag.org/ by guest on August 20, 2018

signaling. EGFR inhibition led to increased UVR-induced keratinocyte apoptosis and skin injury (fig. S4, E to H), resembling results from Langerin-DTA mice and supporting the idea that LCs may limit UVR-induced skin injury by modulating keratinocyte EGFR signaling.

We then examined the effects of LC absence on UVR-induced keratinocyte epidermal EGFR activation. EGFR showed increased phosphorylation by 1 hour after UVR exposure (fig. S4I) (*21*), so we assessed this time point in subsequent experiments. The epidermis from Langerin-DTA mice had a modest reduction in homeostatic EGFR phosphorylation (Fig. 3A), and phosphorylation was not up-regulated after UVR (Fig. 3B). These results suggested that LCs mediated the UVR-induced keratinocyte EGFR activation.

We asked whether the LC-dependent EGFR stimulation was protective for keratinocytes. Treatment of Langerin-DTA mice with heparin-binding EGF-like growth factor (HB-EGF), a potent EGFR ligand (*30*), reduced UVR-induced apoptotic keratinocyte and monocyte accumulation (Fig. 3, C and D). In vitro, adding human LCs or HB-EGF to keratinocytes was similar in limiting UVR-induced apoptosis (Fig. 3E and fig. S5A). Furthermore, small interfering RNA (siRNA)–mediated knockdown of *Egfr* (fig. S5B) or EGFR inhibition in keratinocytes (fig. S5C) abolished the protective effect of LCs (Fig. 3, F and G), whereas EGFR inhibition in LCs did not (fig. S5, D and E). Together, these results suggested that LCs limit UVR-induced keratinocyte apoptosis and skin inflammation by stimulating keratinocyte EGFR.

LC ADAM17 is critical for limiting photosensitivity and is activated by UVR

We asked whether LCs could be a key source of EGFR ligands. Both murine and human LCs expressed multiple EGFR ligands, such as epigen and amphiregulin, which were up-regulated by UVR exposure in murine LCs (Fig. 4, A and B). A disintegrin and metalloprotease 17 (ADAM17) is a membrane-associated metalloprotease that is necessary for the cleavage and activation in cis of all EGFR ligands except EGF and β-cellulin (*31*), the two ligands not expressed or minimally expressed by LCs (Fig. 4, A and B). Murine and human LCs expressed ADAM 17 (fig. S6, A to C). The expression of both EGFR ligands and ADAM17 supported the idea that LCs were potentially capable of directly activating keratinocyte EGFR.

Because LCs expressed multiple EGFR ligands, we assessed the role of LC-derived EGFR ligands by crossing ADAM17$^{flox/flox}$ mice (*32*) with Langerin-Cre$^{+/-}$ mice (*33*) to generate Langerin-Cre$^{+/-}$ADAM17$^{flox/flox}$ mice (LC-Ad17 mice) that have *Adam17* constitutively deleted from LCs (fig. S6D). The Langerin-Cre driver itself had no effect on UVR-induced keratinocyte apoptosis (fig. S6E), so experiments henceforth used Langerin-Cre$^{-/-}$ADAM17$^{flox/flox}$ mice as controls (WT). Although WT and LC-Ad17 mice had comparable

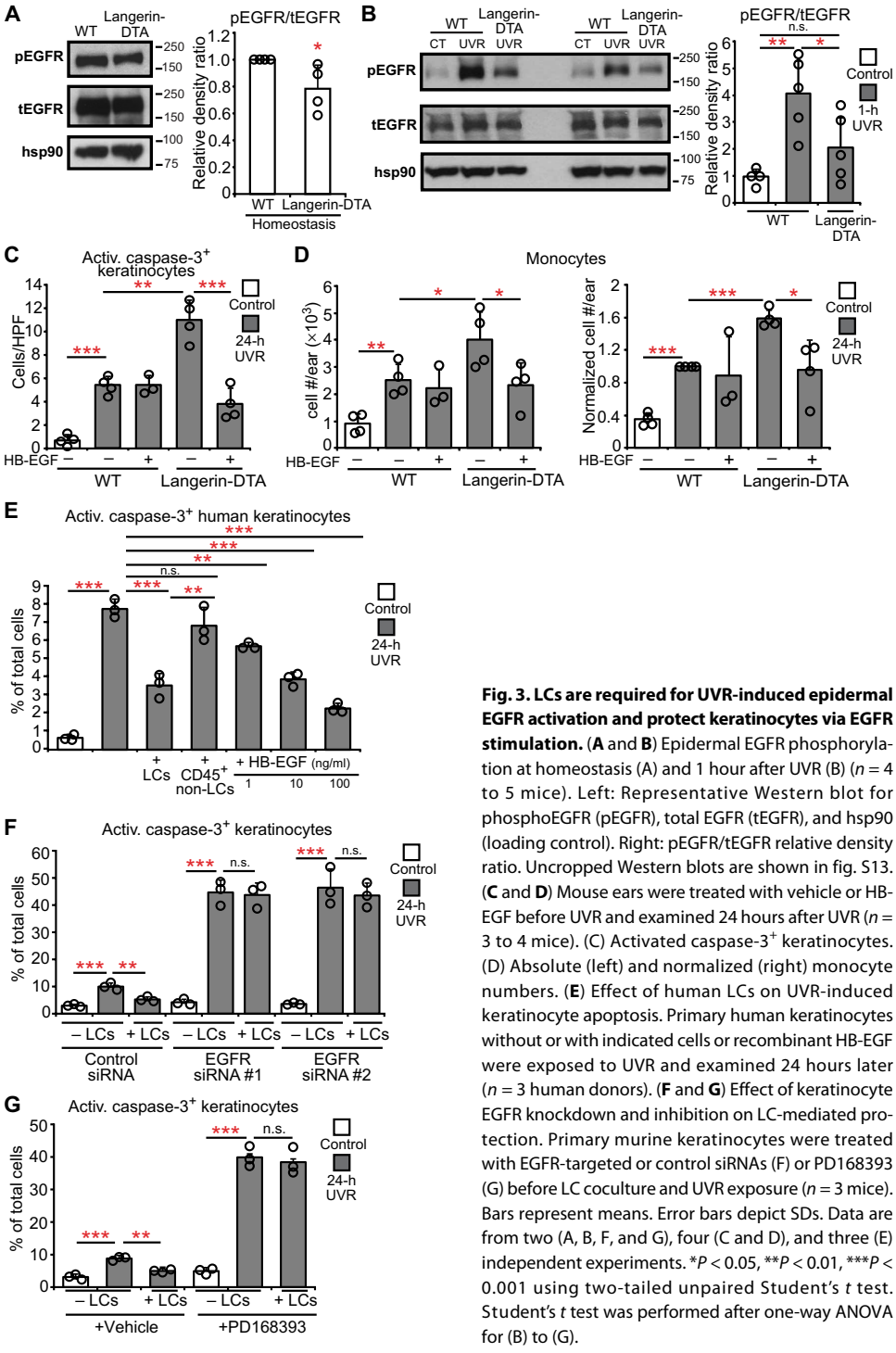

Fig. 3. LCs are required for UVR-induced epidermal EGFR activation and protect keratinocytes via EGFR stimulation. (**A** and **B**) Epidermal EGFR phosphorylation at homeostasis (A) and 1 hour after UVR (B) ($n = 4$ to 5 mice). Left: Representative Western blot for phosphoEGFR (pEGFR), total EGFR (tEGFR), and hsp90 (loading control). Right: pEGFR/tEGFR relative density ratio. Uncropped Western blots are shown in fig. S13. (**C** and **D**) Mouse ears were treated with vehicle or HB-EGF before UVR and examined 24 hours after UVR ($n =$ 3 to 4 mice). (C) Activated caspase-3$^+$ keratinocytes. (D) Absolute (left) and normalized (right) monocyte numbers. (**E**) Effect of human LCs on UVR-induced keratinocyte apoptosis. Primary human keratinocytes without or with indicated cells or recombinant HB-EGF were exposed to UVR and examined 24 hours later ($n = 3$ human donors). (**F** and **G**) Effect of keratinocyte EGFR knockdown and inhibition on LC-mediated protection. Primary murine keratinocytes were treated with EGFR-targeted or control siRNAs (F) or PD168393 (G) before LC coculture and UVR exposure ($n = 3$ mice). Bars represent means. Error bars depict SDs. Data are from two (A, B, F, and G), four (C and D), and three (E) independent experiments. *$P < 0.05$, **$P < 0.01$, ***$P <$ 0.001 using two-tailed unpaired Student's t test. Student's t test was performed after one-way ANOVA for (B) to (G).

Downloaded from http://stm.sciencemag.org/ by guest on August 20, 2018

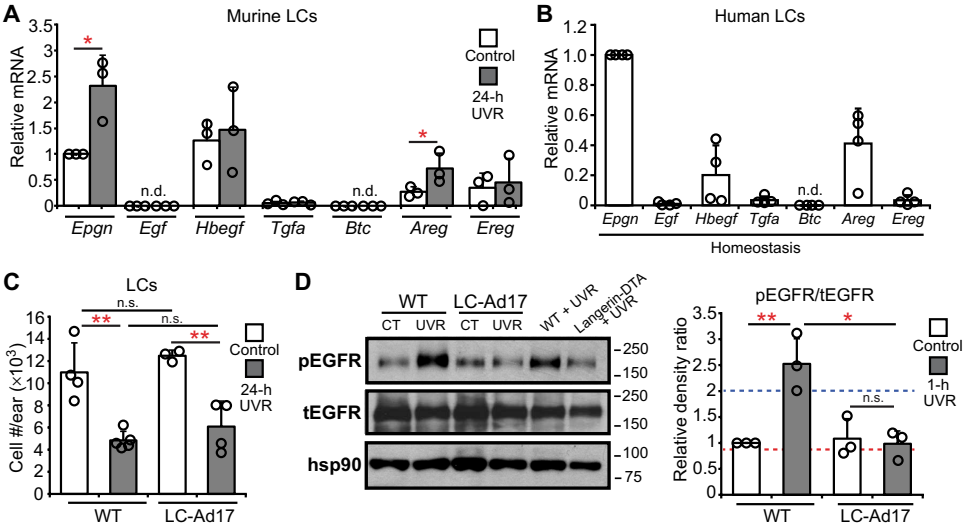

Fig. 4. LCs express EGFR ligands, and LC-derived ADAM17 mediates UVR-induced epidermal EGFR phosphorylation. (**A** and **B**) Murine (A) and human (B) LC EGFR ligand expression (n = 3 to 4 mice or human donors). Murine LCs were sorted from control or UVR-exposed mice. Expression of each ligand was normalized to control murine *Epgn* or human *Epgn* expression. n.d., not detectable. (**C** and **D**) WT and LC-Ad17 mice were treated with UVR and analyzed at indicated time points. (C) LC numbers (n = 3 to 5 mice). (D) Epidermal EGFR phosphorylation. Left: Representative Western blot. Right: pEGFR/tEGFR ratio. Dashed lines are the values for the UVR-exposed WT (blue) and Langerin-DTA (red) mice shown in the blot. Uncropped Western blots are shown in fig. S13. Data are from three (A and B), four (C), and two (D) independent experiments. Bars represent means. Error bars depict SDs. *P < 0.05, **P < 0.01 using two-tailed unpaired Student's t test. Student's t test was performed after one-way ANOVA for (C) and (D).

LC numbers (Fig. 4C), LC-Ad17 mice showed reduced UVR-induced epidermal EGFR phosphorylation (Fig. 4D), suggesting that LC-derived ADAM17 was important for UVR-induced keratinocyte EGFR activation.

We further asked about the importance of LC ADAM17 in protecting the skin. The LC-Ad17 mice showed increased accumulation of apoptotic keratinocytes, monocytes, and monocyte-derived DCs (Fig. 5, A and B, and fig. S6, F and G), blunted epidermal hyperplasia (Fig. 5C), and increased epidermal permeability (Fig. 5D) after UVR exposure. Inducible deletion in LCs (*34*) of ADAM17 in Langerin-Cre-ER$^{+/-}$ ADAM17$^{flox/flox}$ mice also increased UVR-induced keratinocyte apoptosis and monocyte accumulation (fig. S7, A to E). HB-EGF treatment dampened the increased UVR-induced keratinocyte apoptosis and skin inflammation in LC-Ad17 mice (Fig. 5, E and F), supporting the idea that the effect of LC ADAM17 deletion involved EGFR signals. In vitro, ADAM17 deficiency or blockade rendered LCs unable to protect keratinocytes from UVR-induced apoptosis in both murine and human systems (Fig. 5, G and H). These results together strongly supported the idea that LCs limit UVR effects via ADAM17 and stimulating keratinocyte EGFR.

The rapid LC-dependent increase in epidermal EGFR activation with UVR suggested that LC ADAM17 could be activated by UVR. To measure ADAM17 activity, we quantified the level of cell-surface tumor necrosis factor receptor 1 (TNFR1), a substrate for ADAM17 (*31*). Treatment with phorbol 12-myristate 13-acetate (PMA), a known ADAM17 activator (*31*), reduced murine LC TNFR1 in an ADAM17-dependent manner, as expected (Fig. 6A). Similar to PMA, UVR rapidly reduced TNFR1 on both murine and human LCs (Fig. 6, A and B). This effect was abrogated by *Adam17* deletion or ADAM17 blockade (Fig. 6, A and B). These results suggested that ADAM17 on LCs can be rapidly activated by UVR.

To examine whether the UVR-induced ADAM17 activation actually resulted in EGFR ligand cleavage and release, we collected conditioned supernatants from UVR-exposed LCs and assessed how well the supernatants induced EGFR phosphorylation in EGFR-overexpressing A431 indicator cells (fig. S8, A and B). In contrast to supernatants from murine or human LCs that were not exposed to UVR, supernatants from UVR-exposed LCs induced a robust increase in A431 cell EGFR phosphorylation, and *Adam17* deletion or ADAM17 blockade abolished this effect (Fig. 6, C and D). UVR has been shown to activate ADAM17 on keratinocytes (*35*), and UVR exposure also caused murine keratinocytes to release more EGFR ligands, although this effect was less pronounced than that seen in the LCs (fig. S8C). These data further established that UVR can trigger ADAM17 activation on LCs and showed that this activation can result in greater availability of active EGFR ligand. Together, our results show a central role for LCs and LC-derived ADAM17 in vivo and UVR-induced ADAM17 activation on LCs ex vivo, suggesting that there is an LC-keratinocyte axis whereby UVR induces LC ADAM17 activation and consequent EGFR ligand cleavage, leading to increased keratinocyte EGFR activation, which limits UVR-induced keratinocyte apoptosis and skin injury.

The LC-keratinocyte axis is dysfunctional in photosensitive SLE models and human SLE

We asked whether photosensitivity in SLE models, at least in part, reflected dysfunction of this LC-keratinocyte axis. The MRL-*Fas*^{lpr} SLE model is a known photosensitive strain, developing more UVR-induced skin pathology than control Balb/c and/or MRL-MpJ mice (*36*, *37*). UVR induces increased apoptotic keratinocyte accumulation in MRL-*Fas*^{lpr} mice (Fig. 7A) (*36*) along with skin plasma cell accumulation (fig. S9A). Consistent with the possibility of a dysfunctional LC-keratinocyte axis, MRL-*Fas*^{lpr} mice showed reduced UVR-induced EGFR phosphorylation (Fig. 7B).

LC numbers are comparable between MRL-*Fas*^{lpr} mice and Balb/c controls (*38*), and we asked about their ability to protect the skin. MRL-*Fas*^{lpr} LCs showed a trend toward reduced expression of epigen, the most abundantly expressed EGFR ligand, with UVR and reduced expression of epiregulin (fig. S9B), a ligand with relatively low expression (Fig. 4A). *Adam17* mRNA, on the other hand, was reduced in MRL-*Fas*^{lpr} mice by about 70% at homeostasis and after UVR exposure (Fig. 7C). Consistent with the reduced *Adam17* expression, MRL-*Fas*^{lpr} LCs showed no UVR-induced ADAM17 activation as indicated by TNFR1 changes or release of EGFR ligands (fig. S9, C and D). In vitro, MRL-*Fas*^{lpr} LCs did not limit UVR-induced keratinocyte apoptosis (Fig. 7D), whereas control LCs could limit UVR-induced apoptosis of MRL-*Fas*^{lpr} keratinocytes (Fig. 7D), suggesting that LC dysfunction was the critical defect

Downloaded from http://stm.sciencemag.org/ by guest on August 20, 2018

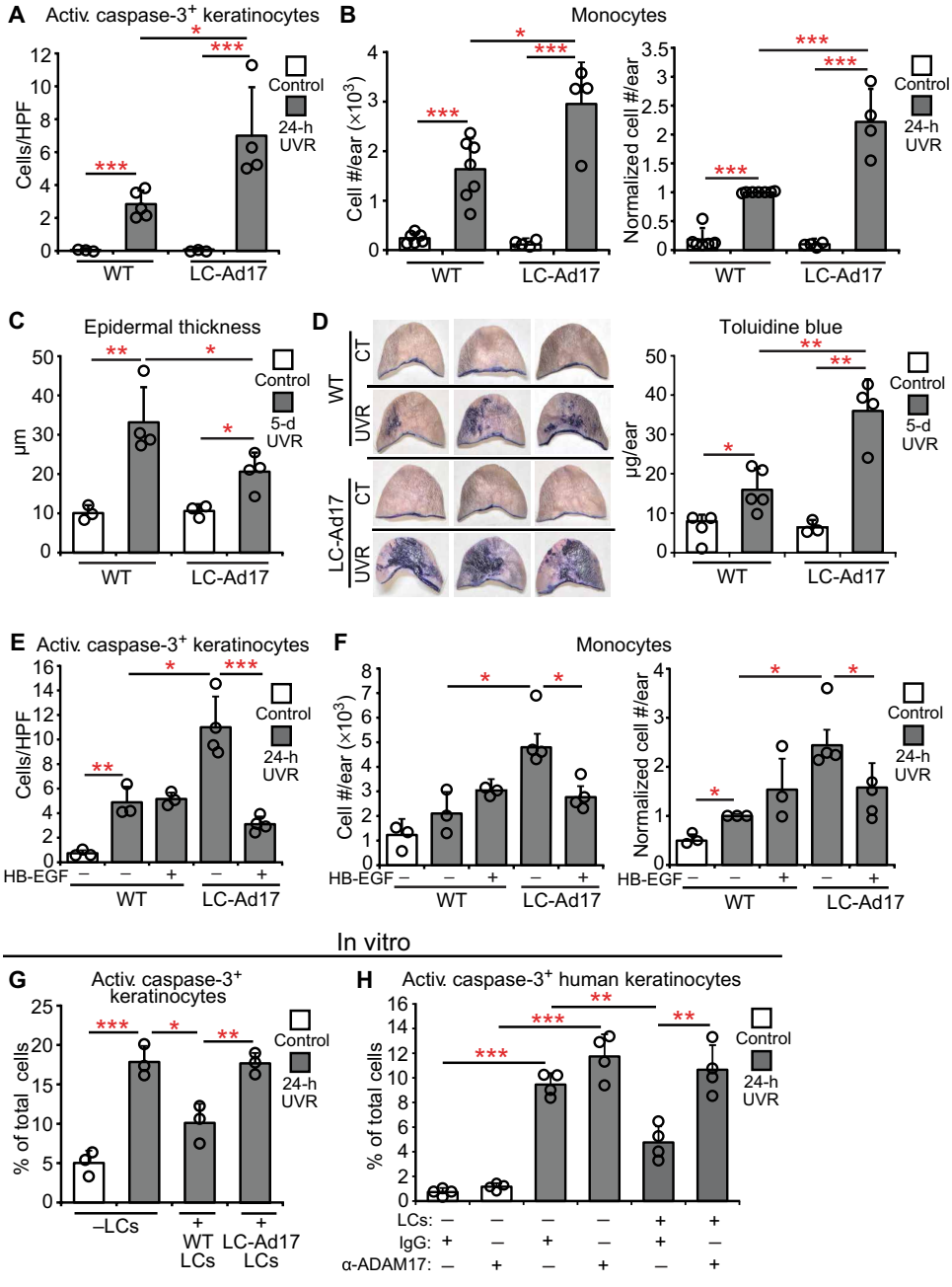

Fig. 5. LC-derived ADAM17 limits UVR-induced keratinocyte apoptosis and skin injury. (**A** to **D**) WT and LC-Ad17 mice were treated with UVR and analyzed at indicated time points. (A) Activated caspase-3$^+$ keratinocytes (n = 3 to 5 mice). (B) Absolute (left) and normalized (right) monocyte numbers (n = 4 to 7 mice). (C) Epidermal thickness (n = 3 to 4 mice). (D) Epidermal permeability (n = 3 to 5 mice). Left: Representative images. Right: Quantification. (**E** and **F**) Vehicle or HB-EGF was applied on the ears before UVR exposure (n = 3 to 4 mice). (E) Activated caspase-3$^+$ keratinocytes. (F) Absolute (left) and normalized (right) monocyte numbers. (**G** and **H**) Effect of LC *Adam17* deletion or ADAM17 blockade on keratinocyte survival in vitro. Murine keratinocytes with LCs from indicated mice (G) and human keratinocytes with control immunoglobulin G (IgG) or anti-ADAM17–treated LCs (H) were exposed to UVR and examined at 24 hours (n = 3 mice, n = 4 human donors). Data are from three (E to G), four (A), two (H), five (B), and one (C and D) independent experiments. Bars represent means (A, B, and D to H) or medians (C). Error bars depict SDs (A, B, and D to H) or interquartile ranges (C). *P < 0.05, **P < 0.01, ***P < 0.001 using two-tailed unpaired Student's t test (A, B, and D to H) or nonparametric nondirectional Mann-Whitney U test after one-way ANOVA (C).

leading to increased UVR sensitivity in MRL-*Fas*^{lpr} mice. These data together suggested that MRL-*Fas*^{lpr} LCs, because of reduced ADAM17 and potentially because of reduced EGFR ligand expression, were unable stimulate epidermal EGFR, thus contributing to photosensitivity.

We also examined the B6.Sle1yaa model of SLE. These mice carry the Sle1 lupus susceptibility locus derived from lupus-prone NZB2410 mice along with the Y chromosome autoimmune accelerator locus whose activity is attributable to Toll-like receptor 7 duplication (*39*). The mice develop lymphadenopathy by 3 months (fig. S10A), splenomegaly and autoantibody production by 4 months, and nephritis by 12 months (*40*). However, the photosensitivity of this model is unknown. Six-week-old B6.Sle1yaa mice did not show increased UVR-induced keratinocyte apoptosis (fig. S10B), but 8- to 12-month-old B6.Sle1yaa mice did (Fig. 7E). Upon multiday UVR treatment, 8- to 12-month-old B6.Sle1yaa mice developed skin lesions as early as 2 days, whereas B6 mice did not (fig. S10C). The skin findings were associated with the presence of plasma cells in the skin (fig. S10D). These results indicated that diseased B6.Sle1yaa mice are photosensitive.

The 8- to 12-month-old B6.Sle1yaa mice also showed reduced UVR-induced epidermal EGFR activation relative to controls (Fig. 7F). LC numbers were unchanged, and only the EGFR ligand amphiregulin was reduced (fig. S10, E and F), but B6.Sle1yaa LCs showed reduced *Adam17* mRNA expression (Fig. 7G). Together, these data suggested that photosensitivity in both SLE models may be attributable, at least in part, to a dysfunctional LC-keratinocyte axis whereby LCs are less able to produce activated EGFR ligands to stimulate keratinocyte EGFR.

We examined human SLE skin for signs of a dysfunctional LC-keratinocyte axis. Nonsun-exposed, nonlesional SLE skin showed decreased LC numbers relative to healthy control skin (Fig. 7H), suggesting an abnormality in LC function and a potential for reduced input of EGFR ligands. Epidermal EGFR phosphorylation was also reduced in SLE skin (Fig. 7I). These data support the idea that the LC-keratinocyte axis is dysfunctional in human SLE.

Downloaded from http://stm.sciencemag.org/ by guest on August 20, 2018

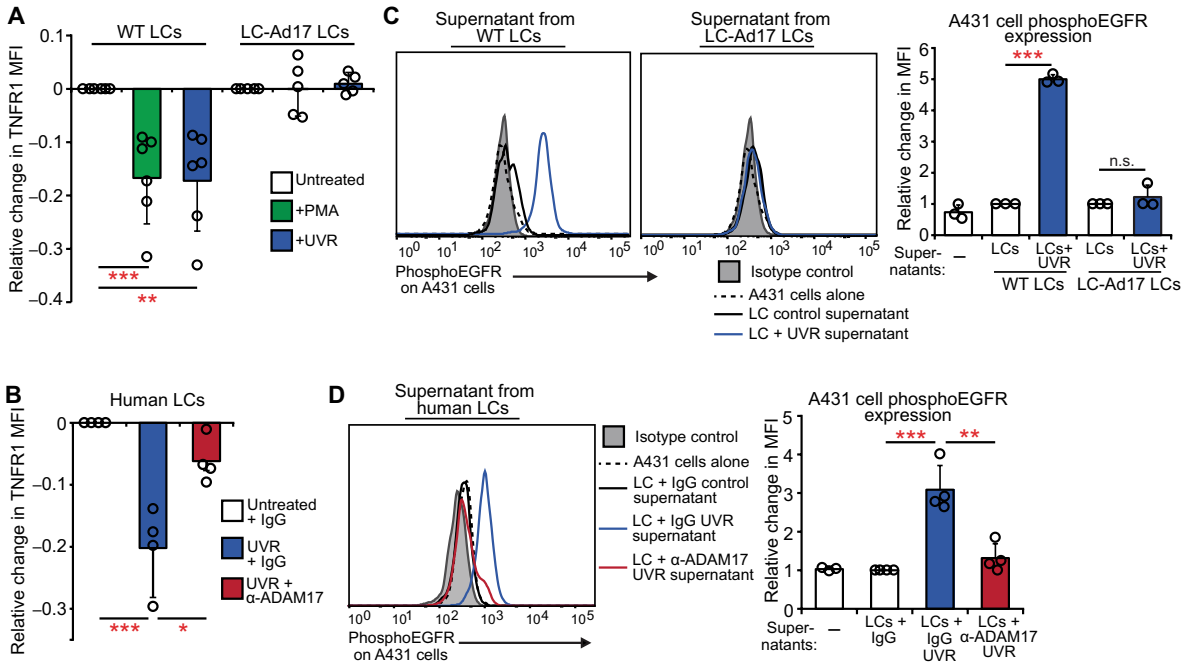

Fig. 6. UVR directly activates LC ADAM17 and EGFR ligand release. (**A** and **B**) Effect of UVR on ADAM17 activity in sorted murine (A) and human (B) LCs as measured by change in TNFR1 mean fluorescence intensity (MFI) 45 min after the indicated treatments. PMA is a positive control ($n = 5$ to 6 mice, $n = 4$ human donors). (**C** and **D**) Conditioned supernatants from murine (C) or human LCs (D) were added to A431 EGFR indicator cells, and phosphoEGFR was measured 10 min later by flow cytometry. Murine LC supernatants were from (A); human LC supernatants were from cells treated similarly to (B), except that the antibody was washed out before UVR (see the Supplementary Materials). Left: Representative histogram. Right: Quantification relative to cells treated with control WT LC supernatants (C) or control IgG-treated LC supernatants (D). Results are from six (A), two (B and D), and three (C) independent experiments. Bars represent means. Error bars depict SDs. *$P < 0.05$, **$P < 0.01$, ***$P < 0.001$ using two-tailed unpaired Student's *t* test after one-way ANOVA.

Topical EGFR ligand reduces photosensitivity in an SLE model

We asked whether EGFR ligand supplementation could reduce photosensitivity in MRL-*Fas*^{lpr} mice. Multiday UVR exposure has been shown to increase complement and immunoglobulin deposition in skin (*36*), and we observed that this regimen also led to ulcerations with a neutrophil-dominant infiltrate (Fig. 8, A to D, and fig. S11, A and B). Topical treatment with HB-EGF (Fig. 8A) reduced the severity of UVR-induced skin lesions (Fig. 8, B to D, and fig. S11, A and B) and monocyte accumulation (Fig. 8E). Topical HB-EGF also reduced germinal center B cells (fig. S11C) and plasma cells (fig. S11D) in skin-draining lymph nodes, suggesting that modulating skin EGFR signaling may affect systemic immunity. These findings suggest that compensating for a dysfunctional LC-keratinocyte axis by providing EGFR ligand can be used as an approach to treating photosensitivity.

DISCUSSION

LCs are best known as antigen-presenting cells, and our findings here establish LCs also as direct modulators of keratinocyte function and skin integrity whereby LCs limit sensitivity to UVR-induced keratinocyte apoptosis and skin injury. The mechanism requires LC expression of ADAM17, the metalloprotease that activates LC-expressed EGFR ligands to stimulate epidermal EGFR. LC abnormalities may contribute to dysfunction of the LC-keratinocyte axis in SLE, leading to photosensitivity, and EGFR ligand supplementation may be an approach to treating photosensitivity (fig. S12).

The LC-keratinocyte axis appears to be a stress survival mechanism. During homeostasis, keratinocyte ADAM17 plays a major role in maintaining skin integrity and barrier function (*23*), and our results indicating that LCs have only a modest role in maintaining epidermal EGFR phosphorylation during homeostasis are consistent with this. In contrast, LCs and LC ADAM17 had an important role in limiting skin injury with UVR, suggesting a scenario in which, in times of stress, keratinocytes require an extra source of EGFR ligands and LCs function as this source. That LC ADAM17 responded more robustly to UVR than keratinocyte ADAM17 further supported a role for LCs in providing a critical source of EGFR ligands in the setting of stress. This role in promoting survival during stress is similar to the role of DCs that we have delineated in inflamed lymph nodes and fibrotic skin (*14*, *15*). Murine LCs are closely related to macrophages in ontogeny but have classical DC functions (*10*). Our findings suggest that LCs behave as DCs in maintaining epidermal integrity in times of stress.

Our model that LCs provide EGFR ligands to stimulate keratinocyte EGFR was supported by the UVR-induced increase in EGFR phosphorylation. In vitro, UVR-induced EGFR phosphorylation has been shown to involve both ligand-induced EGFR kinase activity (*35*, *41*, *42*) and reduction of protein receptor-type phosphatase κ activity (*43*). The inhibition of UVR-induced EGFR phosphorylation by an EGFR tyrosine kinase inhibitor in vivo supports the importance of EGFR kinase activity. Whether LCs also regulate phosphatase activity merits further study.

Our study adds to the recent developments showing rapid EGFR ligand production at barrier surfaces as a protective mechanism.

Downloaded from http://stm.sciencemag.org/ by guest on August 20, 2018

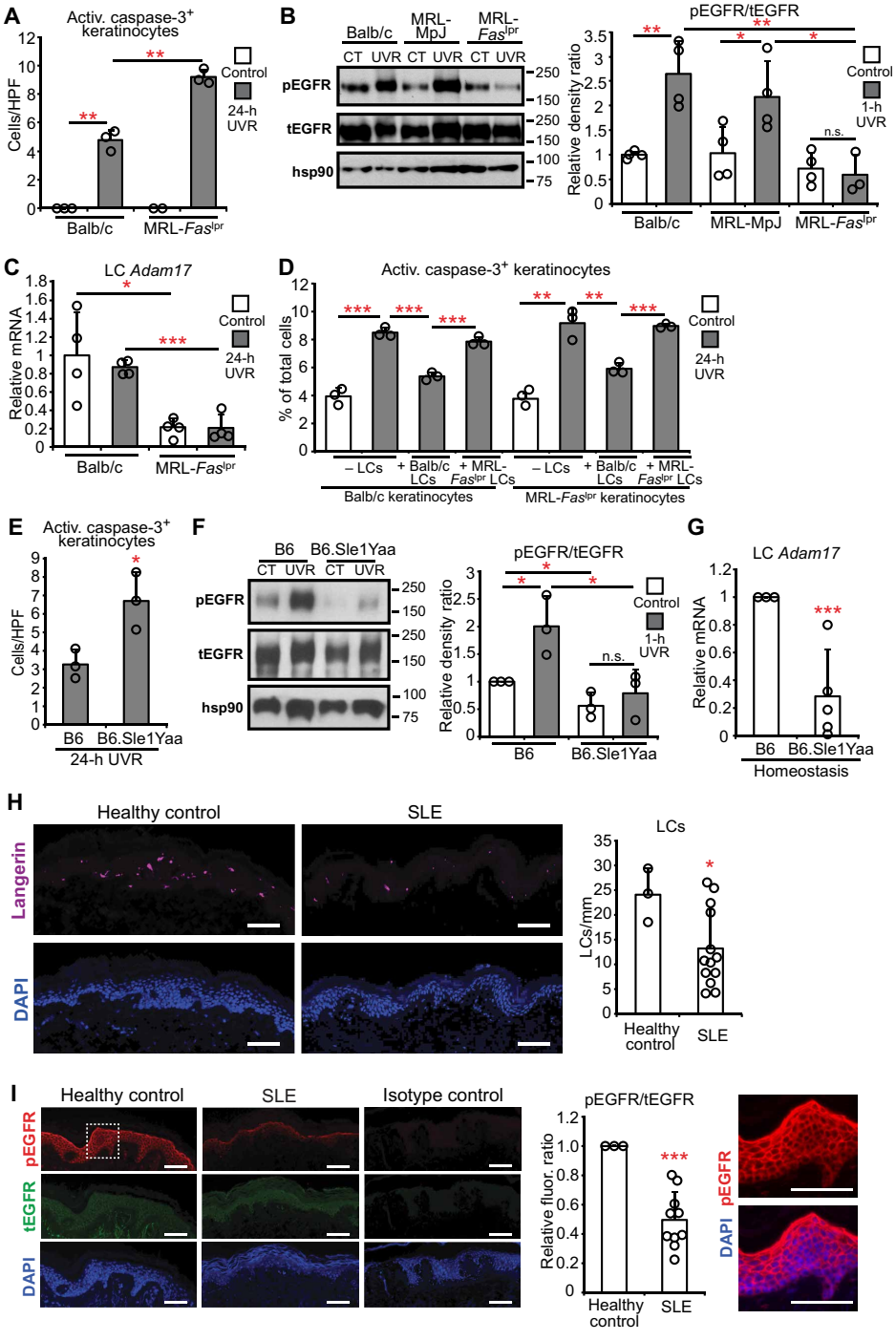

Fig. 7. Photosensitive SLE mouse models and human SLE skin show a dysfunctional LC-keratinocyte axis. WT and MRL-*Fas*^{lpr} ($n = 2$ to 4 mice) (**A** to **C**) or B6.Sle1Yaa mice ($n = 3$ to 5 mice) (**E** to **G**) were treated and examined as indicated. (A and E) Activated caspase-3$^+$ keratinocytes. (B and F) Epidermal EGFR phosphorylation 1 hour after UVR. Left: Representative Western blot. Right: pEGFR/tEGFR ratio. Uncropped Western blots are shown in fig. S13. (C and G) LC *Adam17* expression. (D) Effect of MRL-*Fas*^{lpr} LCs on keratinocyte apoptosis. Balb/c or MRL-*Fas*^{lpr} keratinocytes were exposed to UVR without or with indicated LCs ($n = 3$ mice). (**H** and **I**) LC numbers and epidermal EGFR phosphorylation in human SLE skin ($n = 3$ healthy controls, $n = 10$ to 13 SLE patients). Scale bars, 50 μm. (H) Left: Representative images of anti-Langerin (purple) and DAPI (blue) staining. Right: LC numbers per millimeter of tissue. (I) Left: Representative images of anti-pEGFR (red), anti-tEGFR (green), and DAPI (blue) staining. Middle: Relative pEGFR/tEGFR fluorescence (fluor.) intensity normalized to healthy control skin. Right: Magnified inset from pEGFR and DAPI stain. Data are from three (A, B, D, E, and G to I) and two (C and F) independent experiments. Bars represent means. Error bars depict SDs. *$P < 0.05$, **$P < 0.01$, ***$P < 0.001$ using two-tailed unpaired Student's *t* test. Student's *t* test was performed after one-way ANOVA for (A) to (D) and (F).

Regulatory T cells and group 2 innate lymphoid cells have recently been shown to be critical sources of the EGFR ligand amphiregulin in protecting lung and colonic epithelium, respectively, during inflammation (*44*, *45*). In these models, amphiregulin expression was induced within days by alarmins from the injured tissues. In contrast, LCs were "immediate responders," because LC-dependent epidermal phosphoEGFR up-regulation occurred by 1 hour after UVR in vivo, and UVR could act directly on LCs to activate LC ADAM17 ex vivo. Whether injured keratinocyte signals induce the up-regulation of LC epigen and amphiregulin at 24 hours and whether LCs are unique among immune cells in direct activation of ADAM17 are unknown. However, our study and that of others' together suggest that there are distinct immediate versus early layers of regulation to protect barrier surfaces.

Hatakeyama *et al.* (*46*) recently suggested that LCs help to resolve UVR-induced skin inflammation at day 5 and later after UVR exposure by ingesting and clearing apoptotic keratinocytes. We show distinct findings, focusing on immediate events after UVR exposure. Furthermore, we detected essentially no activated caspase-3$^+$ Langerin$^+$ cells at 24 hours after exposure in WT mice and in LC-keratinocyte cocultures, suggesting that LC phagocytosis of apoptotic keratinocytes was minimal both in vivo and in vitro. Thus, although we do not rule out a role for LCs in clearing apoptotic keratinocytes at later time points, our study firmly establishes a role for LCs in limiting keratinocyte apoptosis early on.

Our study also suggested that LCs limit monocyte recruitment to the UVR-exposed skin and that accumulated monocytes contribute to increased epidermal permeability. UVR has long been noted to deplete LCs from the skin, and this depletion correlated with myeloid cell accumulation (*47*). Our results would suggest that the UVR-mediated depletion of LCs caused the myeloid cell accumulation and that stronger or chronic UVR exposure would further deplete LCs, leading to greater myeloid cell accumulation. EGFR activity has been shown to limit keratinocyte CCL2 expression (*7*), but the extent to which LCs alter chemokine expression by keratinocytes, fibroblasts, or endothelial cells needs to be examined

Downloaded from http://stm.sciencemag.org/ by guest on August 20, 2018

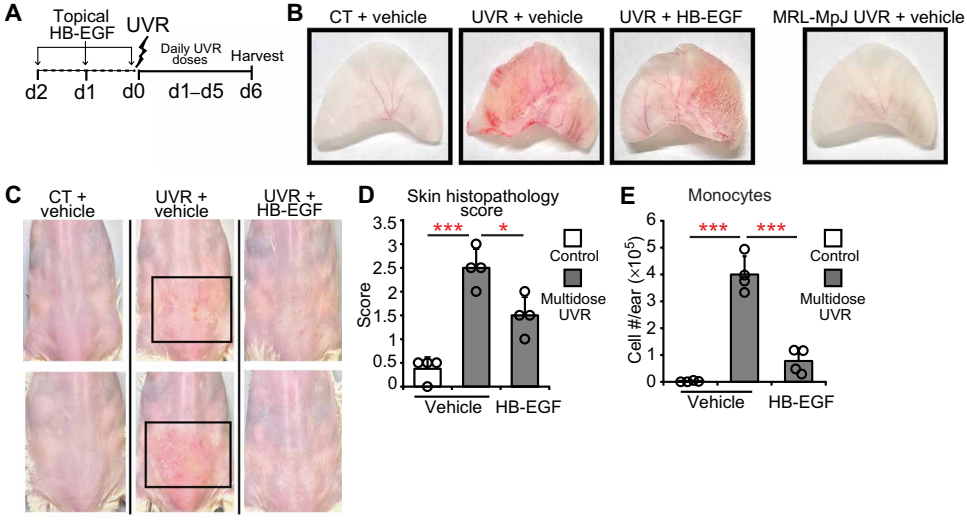

Fig. 8. Topical EGFR ligand reduces photosensitivity. (**A**) Experimental scheme for (**B**) to (**E**) ($n = 4$ mice). MRL-*Fas*^{lpr} mouse ears and back skin were topically treated with HB-EGF for 2 days before and on the first day of UVR exposure and examined 24 hours after the final exposure. (B) Representative images of ears. The MRL-MpJ ear represents a non-SLE control. (C) Representative images of back skin; boxes outline lesional areas. Magnified images of back skin are shown in fig. S11. (D) Ear histopathology score. (E) Absolute monocyte numbers. (B to E) Data are from three independent experiments. Bars represent means. Error bars depict SDs. *$P < 0.05$, ***$P < 0.001$ using two-tailed unpaired Student's *t* test after one-way ANOVA.

more directly in future studies. Sontheimer *et al.* (*48*) recently showed that monocytes may be a major source of type I interferon a few days after UVR exposure, and it would be interesting to understand whether type I interferon increased epidermal permeability. Because UVR is also associated with immune suppression in healthy humans but increased autoimmunity in SLE patients (*1*, *47*), it will be interesting to understand whether monocyte and monocyte-derived cells participate in differentially modulating immunity after UVR exposure in healthy and lupus erythematosus patients.

Our study is relevant for understanding photosensitivity in human disease in several ways. First, we showed that the LC-keratinocyte axis is dysfunctional in two SLE models, and the reduced EGFR phosphorylation in human SLE skin suggested that this axis may be dysfunctional and contribute to photosensitivity in human SLE. LC numbers were reduced in human SLE skin, and whether the reduced epidermal EGFR phosphorylation reflected the LC reduction, or other defects such as reduced LC ADAM17 or EGFR ligand expression, remains to be determined. Although LC-independent keratinocyte-intrinsic dysfunction may also lead to reduced epidermal EGFR phosphorylation and will need to be considered, the reduced LC numbers suggest failure of LC development or survival or perhaps increased migration to draining lymph nodes and suggest that LCs may be dysfunctional in human SLE. Second, our data showed that LCs protected at least UVA-mediated skin injury. Because sunlight is composed primarily of UVA (*49*), our data are relevant for better understanding the mechanisms that protect against the effects of sunlight exposure in lupus patients. Further understanding of LC function and regulation in SLE will be interesting, as will understanding whether there are similar defects in photosensitivity associated with other disorders (*3*).

There are a few limitations of this study. Although epidermal EGFR phosphorylation is reduced in human SLE skin, we do not yet know whether human SLE LCs are less able to provide activated EGFR ligands or protect keratinocytes from UVR. We also do not yet understand how UVR activated ADAM17 or how LCs are dysregulated in the SLE models.

Our data suggest that topical EGFR stimulation could be a treatment to prevent the development of photosensitive cutaneous lesions in lupus erythematosus. The reduction in lymph node B cell responses with HB-EGF suggests that EGFR stimulation could also improve the systemic aspects of photosensitivity in SLE. Although the potential for carcinogenesis should be considered (*50*), topical EGF is being investigated for rashes associated with the use of EGFR inhibitors to treat lung cancer patients who are most likely immunocompromised (CinicalTrials.gov; trials NCT03051880 and NCT03047863) (*51*). Furthermore, in mouse models of colitis-associated cancer, EGFR inhibited tumor development, likely by improving epidermal function and reducing inflammation (*52*). Our findings suggest that EGFR-stimulating agents should be investigated for photosensitivity in lupus erythematosus and potentially other autoimmune and dermatologic conditions.

MATERIALS AND METHODS

Study design

Controlled experiments were designed using mouse models, in vitro systems, and human skin. Animals were randomly assigned to experimental groups. Sample sizes were determined on the basis of previously published experiments using similar tissues and assays (*14*, *15*). No data were excluded, each experiment was performed with at least three biological replicates, and all data were reliably reproduced. Investigators were not blinded to group allocation during experiments and data acquisition. During data analysis, investigators were not blinded for flow cytometry, Western blot, epidermal permeability, and mRNA experiments but were blinded for histology/immunofluorescence and lesion measurements. Sample numbers and numbers of independent experiments are included in each figure legend. Each symbol in figures represents one mouse, human, or biological replicate. List of primary antibodies are in table S1 and secondary antibodies are in table S2. Primary data are included in table S3.

UVR treatments

In vivo, four FS40T12 sunlamps that emit UVA and UVB at a 40:60 ratio (*20*) were used as the UVR source. We determined 1000 J/m^2 UVR to be the minimal dose that caused visible dilation in the ears of C57BL/6J mice at 24 hours and used this dose for all experiments unless otherwise indicated. For multidose experiments with Langerin-DTA mice, mice were shaved 24 hours before the first UVR exposure. SLE model mice were shaved 24 hours before the first UVR exposure and then exposed to UVR (500 J/m^2) for six consecutive days for

Downloaded from http://stm.sciencemag.org/ by guest on August 20, 2018

lesion development experiments. In vitro, mouse and human primary keratinocytes and LCs were exposed to UVR (500 J/m^2) with the same UVR lamps as above.

Statistical analyses

For analyses of experiments with more than two groups, one-way ANOVA was initially used to examine differences among groups. For data that were normally distributed according to the Shapiro-Wilkes test, the ANOVA was followed by the two-tailed unpaired Student's *t* test to assess differences between two particular groups. For data that were not normally distributed, the nondirectional nonparametric Mann-Whiney *U* test was used to determine differences between two groups. For analyses of experiments with only two groups, we determined the distribution with the Shapiro-Wilkes test and then used the appropriate statistical test for comparison. The statistical test and measure of uncertainty used for each figure are included in the figure legend.

SUPPLEMENTARY MATERIALS

www.sciencetranslationalmedicine.org/cgi/content/full/10/454/eaap9527/DC1
Materials and Methods
Fig. S1. Additional features of LC-mediated protection from UVR-induced keratinocyte apoptosis and skin injury.
Fig. S2. The role of accumulated monocytes and monocyte-derived DCs in UVR-induced skin injury.
Fig. S3. Additional features of LC-mediated protection of keratinocytes in vitro.
Fig. S4. Mice treated with EGFR inhibitor resemble Langerin-DTA mice and timing of epidermal EGFR activation after UVR exposure.
Fig. S5. Effect of human LCs on human keratinocytes without UVR and further characterization of in vitro LC-keratinocyte EGFR signaling.
Fig. S6. Characterization of mouse and human ADAM17 expression, LC-Ad17 mice, and Langerin-Cre mice.
Fig. S7. Effects of inducible ADAM17 deletion in LCs.
Fig. S8. Validation of EGFR ligand release assay and characterization of keratinocyte EGFR ligand release.
Fig. S9. Photosensitive MRL-*Fas*^{lpr} mice have more skin plasma cells and reduced LC EGFR ligand expression, LC ADAM17 activity, and LC EGFR ligand release.
Fig. S10. B6.Sle1yaa mice exhibit photosensitivity and characterization of EGFR ligand expression by their LCs.
Fig. S11. EGFR ligand application reduces the severity of UVR-induced skin lesions and lymph node B cell responses in SLE model mice.
Fig. S12. Model of protective LC-keratinocyte axis and dysfunction of this axis in lupus photosensitivity.
Fig. S13. Uncropped Western blot images.
Table S1. List of primary antibodies.
Table S2. Secondary antibodies and other staining reagents.
Table S3. Primary data.
Reference (*53*)

REFERENCES AND NOTES

1. M. K. Kuechle, K. B. Elkon, Shining light on lupus and UV. *Arthritis Res. Ther.* **9**, 101 (2007).
2. B. F. Chong, V. P. Werth, in *Dubois' Lupus Erythematosus and Related Syndromes*, B. H. Hahn, Ed. (W.B. Saunders, ed. 8, 2013), pp. 319–332.
3. T. P. Millard, J. L. M. Hawk, Photosensitivity disorders: Cause, effect, and management. *Am. J. Clin. Dermatol.* **3**, 239–246 (2002).
4. T. D. Golan, K. B. Elkon, A. E. Gharavi, J. G. Krueger, Enhanced membrane binding of autoantibodies to cultured keratinocytes of systemic lupus erythematosus patients after ultraviolet B/ultraviolet A irradiation. *J. Clin. Invest.* **90**, 1067–1076 (1992).
5. A. Kuhn, J. Wenzel, H. Weyd, Photosensitivity, apoptosis, and cytokines in the pathogenesis of lupus erythematosus: A critical review. *Clin. Rev. Allergy Immunol.* **47**, 1–15 (2014).
6. E. Reefman, M. C. J. M. de Jong, H. Kuiper, M. F. Jonkman, P. C. Limburg, C. G. Kallenberg, M. Bijl, Is disturbed clearance of apoptotic keratinocytes responsible for UVB-induced inflammatory skin lesions in systemic lupus erythematosus? *Arthritis Res. Ther.* **8**, R156 (2006).
7. B. M. Lichtenberger, P. A. Gerber, M. Holcmann, B. A. Buhren, N. Amberg, V. Smolle, H. Schrumpf, E. Boelke, P. Ansari, C. Mackenzie, A. Wollenberg, A. Kislat, J. W. Fischer, K. Rock, J. Harder, J. M. Schröder, B. Homey, M. Sibilia, Epidermal EGFR controls cutaneous host defense and prevents inflammation. *Sci. Transl. Med.* **5**, 199ra111 (2013).
8. D. Raj, D. E. Brash, D. Grossman, Keratinocyte apoptosis in epidermal development and disease. *J. Invest. Dermatol.* **126**, 243–257 (2006).
9. S. W. Kashem, M. Haniffa, D. H. Kaplan, Antigen-presenting cells in the skin. *Annu. Rev. Immunol.* **35**, 469–499 (2017).
10. T. Doebel, B. Voisin, K. Nagao, Langerhans cells—The macrophage in dendritic cell clothing. *Trends Immunol.* 817–828 (2017).
11. R. D. Sontheimer, P. R. Bergstresser, Epidermal Langerhans cell involvement in cutaneous lupus erythematosus. *J. Invest. Dermatol.* **79**, 237–243 (1982).
12. L. L. Teichmann, M. L. Ols, M. Kashgarian, B. Reizis, D. H. Kaplan, M. J. Shlomchik, Dendritic cells in lupus are not required for activation of T and B cells but promote their expansion, resulting in tissue damage. *Immunity* **33**, 967–978 (2010).
13. J. K. King, R. L. Philips, A. U. Eriksson, P. J. Kim, R. C. Halder, D. J. Lee, R. R. Singh, Langerhans cells maintain local tissue tolerance in a model of systemic autoimmune disease. *J. Immunol.* **195**, 464–476 (2015).
14. J. J. Chia, T. Zhu, S. Chyou, D. C. Dasoveanu, C. Carballo, S. Tian, C. M. Magro, S. Rodeo, R. F. Spiera, N. H. Ruddle, T. E. McGraw, J. L. Browning, R. Lafyatis, J. K. Gordon, T. T. Lu, Dendritic cells maintain dermal adipose–derived stromal cells in skin fibrosis. *J. Clin. Invest.* **126**, 4331–4345 (2016).
15. V. Kumar, D. C. Dasoveanu, S. Chyou, T.-C. Tzeng, C. Rozo, Y. Liang, W. Stohl, Y.-X. Fu, N. H. Ruddle, T. T. Lu, A dendritic-cell-stromal axis maintains immune responses in lymph nodes. *Immunity* **42**, 719–730 (2015).
16. S. Ivanov, J. P. Scallan, K.-W. Kim, K. Werth, M. W. Johnson, B. T. Saunders, P. L. Wang, E. L. Kuan, A. C. Straub, M. Ouhachi, E. G. Weinstein, J. W. Williams, C. Briseño, M. Colonna, B. E. Isakson, E. L. Gautier, R. Förster, M. J. Davis, B. H. Zinselmeyer, G. J. Randolph, CCR7 and IRF4-dependent dendritic cells regulate lymphatic collecting vessel permeability. *J. Clin. Invest.* **126**, 1581–1591 (2016).
17. J. L. Astarita, V. Cremasco, J. Fu, M. C. Darnell, J. R. Peck, J. M. Nieves-Bonilla, K. Song, Y. Kondo, M. C. Woodruff, A. Gogineni, L. Onder, B. Ludewig, R. M. Weimer, M. C. Carroll, D. J. Mooney, L. Xia, S. J. Turley, The CLEC-2-podoplanin axis controls the contractility of fibroblastic reticular cells and lymph node microarchitecture. *Nat. Immunol.* **16**, 75–84 (2015).
18. S. E. Acton, A. J. Farrugia, J. L. Astarita, D. Mourão-Sá, R. P. Jenkins, E. Nye, S. Hooper, J. van Blijswijk, N. C. Rogers, K. J. Snelgrove, I. Rosewell, L. F. Moita, G. Stamp, S. J. Turley, E. Sahai, C. Reis e Sousa, Dendritic cells control fibroblastic reticular network tension and lymph node expansion. *Nature* **514**, 498–502 (2014).
19. D. H. Kaplan, M. C. Jenison, S. Saeland, W. D. Shlomchik, M. J. Shlomchik, Epidermal Langerhans cell-deficient mice develop enhanced contact hypersensitivity. *Immunity* **23**, 611–620 (2005).
20. L. Polla, R. Margolis, C. Goulston, J. A. Parrish, R. D. Granstein, Enhancement of the elicitation phase of the murine contact hypersensitivity response by prior exposure to local ultraviolet radiation. *J. Invest. Dermatol.* **86**, 13–17 (1986).
21. T. B. El-Abaseri, S. Putta, L. A. Hansen, Ultraviolet irradiation induces keratinocyte proliferation and epidermal hyperplasia through the activation of the epidermal growth factor receptor. *Carcinogenesis* **27**, 225–231 (2006).
22. A. Haratake, Y. Uchida, M. Schmuth, O. Tanno, R. Yasuda, J. H. Epstein, P. M. Elias, W. M. Holleran, UVB-induced alterations in permeability barrier function: Roles for epidermal hyperproliferation and thymocyte-mediated response. *J. Invest. Dermatol.* **108**, 769–775 (1997).
23. C.-W. Franzke, C. Cobzaru, A. Triantafyllopoulou, S. Löffek, K. Horiuchi, D. W. Threadgill, T. Kurz, N. van Rooijen, L. Bruckner-Tuderman, C. P. Blobel, Epidermal ADAM17 maintains the skin barrier by regulating EGFR ligand–dependent terminal keratinocyte differentiation. *J. Exp. Med.* **209**, 1105–1119 (2012).
24. S. Tamoutounour, M. Guilliams, F. Montanana Sanchis, H. Liu, D. Terhorst, C. Malosse, E. Pollet, L. Ardouin, H. Luche, C. Sanchez, M. Dalod, B. Malissen, S. Henri, Origins and functional specialization of macrophages and of conventional and monocyte-derived dendritic cells in mouse skin. *Immunity* **39**, 925–938 (2013).
25. T. M. Hohl, A. Rivera, L. Lipuma, A. Gallegos, C. Shi, M. Mack, E. G. Pamer, Inflammatory monocytes facilitate adaptive CD4 T cell responses during respiratory fungal infection. *Cell Host Microbe* **6**, 470–481 (2009).
26. J. L. Doerner, J. Wen, Y. Xia, K. B. Paz, D. Schairer, L. Wu, S. A. Chalmers, P. Izmirly, J. S. Michaelson, L. C. Burkly, A. J. Friedman, C. Putterman, TWEAK/Fn14 signaling involvement in the pathogenesis of cutaneous disease in the MRL/lpr model of spontaneous lupus. *J. Invest. Dermatol.* **135**, 1986–1995 (2015).
27. M. S. Iordanov, R. J. Choi, O. P. Ryabinina, T.-H. Dinh, R. K. Bright, B. E. Magun, The UV (Ribotoxic) stress response of human keratinocytes involves the unexpected uncoupling of the ras-extracellular signal-regulated kinase signaling cascade from the activated epidermal growth factor receptor. *Mol. Cell. Biol.* **22**, 5380–5394 (2002).

Downloaded from http://stm.sciencemag.org/ by guest on August 20, 2018

28. F. Mascia, G. Lam, C. Keith, C. Garber, S. M. Steinberg, E. Kohn, S. H. Yuspa, Genetic ablation of epidermal EGFR reveals the dynamic origin of adverse effects of anti-EGFR therapy. *Sci. Transl. Med.* **5**, 199ra110 (2013).
29. D. W. Fry, A. J. Bridges, W. A. Denny, A. Doherty, K. D. Greis, J. L. Hicks, K. E. Hook, P. R. Keller, W. R. Leopold, J. A. Loo, D. J. McNamara, J. M. Nelson, V. Sherwood, J. B. Smaill, S. Trumpp-Kallmeyer, E. M. Dobrusin, Specific, irreversible inactivation of the epidermal growth factor receptor and erbB2, by a new class of tyrosine kinase inhibitor. *Proc. Natl. Acad. Sci. U.S.A.* **95**, 12022–12027 (1998).
30. T. Ronan, J. L. Macdonald-Obermann, L. Huelsmann, N. J. Bessman, K. M. Naegle, L. J. Pike, Different epidermal growth factor receptor (EGFR) agonists produce unique signatures for the recruitment of downstream signaling proteins. *J. Biol. Chem.* **291**, 5528–5540 (2016).
31. J. Scheller, A. Chalaris, C. Garbers, S. Rose-John, ADAM17: A molecular switch to control inflammation and tissue regeneration. *Trends Immunol.* **32**, 380–387 (2011).
32. K. Horiuchi, T. Kimura, T. Miyamoto, H. Takaishi, Y. Okada, Y. Toyama, C. P. Blobel, Cutting edge: TNF-α-converting enzyme (TACE/ADAM17) inactivation in mouse myeloid cells prevents lethality from endotoxin shock. *J. Immunol.* **179**, 2686–2689 (2007).
33. D. H. Kaplan, M. O. Li, M. C. Jenison, W. D. Shlomchik, R. A. Flavell, M. J. Shlomchik, Autocrine/paracrine TGFβ1 is required for the development of epidermal Langerhans cells. *J. Exp. Med.* **204**, 2545–2552 (2007).
34. A. Bobr, B. Igyarto, K. M. Haley, M. O. Li, R. A. Flavell, D. H. Kaplan, Autocrine/paracrine TGF-β1 inhibits Langerhans cell migration. *Proc. Natl. Acad. Sci. U.S.A.* **109**, 10492–10497 (2012).
35. B. Singh, M. Schneider, P. Knyazev, A. Ullrich, UV-induced EGFR signal transactivation is dependent on proligand shedding by activated metalloproteases in skin cancer cell lines. *Int. J. Cancer* **124**, 531–539 (2009).
36. J. Menke, M.-Y. Hsu, K. T. Byrne, J. A. Lucas, W. A. Rabacal, B. P. Croker, X.-H. Zong, E. R. Stanley, V. R. Kelley, Sunlight triggers cutaneous lupus through a (CSF-1)-dependent mechanism in MRL-*Fas*^{lpr} mice. *J. Immunol.* **181**, 7367–7379 (2008).
37. Y. Horiguchi, F. Furukawa, G. Ohshio, T. Horio, S. Imamura, Effects of ultraviolet light irradiation on the skin of MRL/l mice. *Arch. Dermatol. Res.* **279**, 478–483 (1987).
38. A. U. Eriksson, R. R. Singh, Cutting edge: Migration of Langerhans dendritic cells is impaired in autoimmune dermatitis. *J. Immunol.* **181**, 7468–7472 (2008).
39. P. Pisitkun, J. A. Deane, M. J. Difilippantonio, T. Tarasenko, A. B. Satterthwaite, S. Bolland, Autoreactive B cell responses to RNA-related antigens due to *TLR7* gene duplication. *Science* **312**, 1669–1672 (2006).
40. L. Morel, B. P. Croker, K. R. Blenman, C. Mohan, G. Huang, G. Gilkeson, E. K. Wakeland, Genetic reconstitution of systemic lupus erythematosus immunopathology with polycongenic murine strains. *Proc. Natl. Acad. Sci. U.S.A.* **97**, 6670–6675 (2000).
41. R. P. Huang, J. X. Wu, Y. Fan, E. D. Adamson, UV activates growth factor receptors via reactive oxygen intermediates. *J. Cell Biol.* **133**, 211–220 (1996).
42. C. Sachsenmaier, A. Radler-Pohl, R. Zinck, A. Nordheim, P. Herrlich, H. J. Rahmsdorf, Involvement of growth factor receptors in the mammalian UVC response. *Cell* **78**, 963–972 (1994).
43. Y. Xu, Y. Shao, J. J. Voorhees, G. J. Fisher, Oxidative inhibition of receptor-type protein-tyrosine phosphatase κ by ultraviolet irradiation activates epidermal growth factor receptor in human keratinocytes. *J. Biol. Chem.* **281**, 27389–27397 (2006).
44. L. A. Monticelli, L. C. Osborne, M. Noti, S. V. Tran, D. M. W. Zaiss, D. Artis, IL-33 promotes an innate immune pathway of intestinal tissue protection dependent on amphiregulin-EGFR interactions. *Proc. Natl. Acad. Sci. U.S.A.* **112**, 10762–10767 (2015).
45. N. Arpaia, J. A. Green, B. Moltedo, A. Arvey, S. Hemmers, S. Yuan, P. M. Treuting, A. Y. Rudensky, A distinct function of regulatory T cells in tissue protection. *Cell* **162**, 1078–1089 (2015).
46. M. Hatakeyama, A. Fukunaga, K. Washio, K. Taguchi, Y. Oda, K. Ogura, C. Nishigori, Anti-inflammatory role of Langerhans cells and apoptotic keratinocytes in ultraviolet-B–induced cutaneous inflammation. *J. Immunol.* 2937–2947 (2017).
47. K. D. Cooper, L. Oberhelman, T. A. Hamilton, O. Baadsgaard, M. Terhune, G. LeVee, T. Anderson, H. Koren, UV exposure reduces immunization rates and promotes tolerance to epicutaneous antigens in humans: Relationship to dose, CD1a-DR+ epidermal macrophage induction, and Langerhans cell depletion. *Proc. Natl. Acad. Sci.U.S.A.* **89**, 8497–8501 (1992).
48. C. Sontheimer, D. Liggitt, K. B. Elkon, Ultraviolet B irradiation causes stimulator of interferon genes–dependent production of protective type I interferon in mouse skin by recruited inflammatory monocytes. *Arthritis Rhematol.* **69**, 826–836 (2017).
49. N. Kollias, E. Ruvolo Jr., R. M. Sayre, The value of the ratio of UVA to UVB in sunlight. *Photochem. Photobiol.* **87**, 1474–1475 (2011).
50. P. Uribe, S. Gonzalez, Epidermal growth factor receptor (EGFR) and squamous cell carcinoma of the skin: Molecular bases for EGFR-targeted therapy. *Pathol. Res. Pract.* **207**, 337–342 (2011).
51. J. U. Shin, J. H. Park, B.-C. Cho, J. H. Lee, Treatment of epidermal growth factor receptor inhibitor-induced acneiform eruption with topical recombinant human epidermal growth factor. *Dermatology* **225**, 135–140 (2012).
52. P. E. Dubé, F. Yan, S. Punit, N. Girish, S. J. McElroy, M. K. Washington, D. B. Polk, Epidermal growth factor receptor inhibits colitis-associated cancer in mice. *J. Clin. Invest.* **122**, 2780–2792 (2012).
53. P. M. Izmirly, M. Shvartsbeyn, S. Meehan, A. Franks, A. Braun, E. Ginzler, S. X. Xu, H. Yee, T. Rivera, C. Esmon, L. Barisoni, J. T. Merrill, J. P. Buyon, R. M. Clancy, Dysregulation of the microvasculature in nonlesional non-sun-exposed skin of patients with lupus nephritis. *J. Rheumatol.* **39**, 510–515 (2012).

Acknowledgments: We thank I. Rogatsky's and A. Pernis's laboratories for helpful discussions and J. Szymonifka for help with the statistical analysis. **Funding:** This work was supported by NIH MSTP T32GM007739 to the Weill Cornell/Rockefeller/Sloan-Kettering Tri-Institutional MD-PhD Program (to W.D.S.), NIH T32AR071302-01 to the Hospital for Special Surgery Research Institute Rheumatology Training Program (to W.D.S.), and NIH R01AI079178, Alliance for Lupus Research Target Identification grant, Lupus Research Institute Novel Research Grant, St. Giles Foundation, and an O'Neill Foundation grant from the Barbara Volcker Center for Women and Rheumatic Diseases (all to T.T.L.). The research was supported by the NIH Office of the Director grant S10OD019986 to Hospital for Special Surgery. The content of this work is solely the responsibility of the authors and does not necessarily represent official NIH views. **Author contributions:** W.D.S., S.C., A.R., S.S., and D.C.D. designed, performed, and interpreted experiments. T.P. and C.M.M. interpreted experiments. D.H.K., J.E.S., X.Q., E.G.P., B.J.M., J.W.Y., and C.P.B. provided reagents. P.M.I. and R.M.C. provided patient skin samples and slides. S.S., B.J.M., and J.W.Y. provided and processed fresh human skin samples. R.D.G., M.A.L., D.H.K., J.E.S., J.W.Y., R.M.C., and C.P.B. provided critical input during manuscript development and writing. T.T.L. designed, supervised, and interpreted experiments. W.D.S. and T.T.L. wrote the paper. **Competing interests:** The authors declare that they have no competing financial interests. **Data and materials availability:** No data sets were generated. All relevant data supporting the findings of this study are available within the paper and its Supplementary Materials.

Submitted 20 September 2017
Accepted 13 July 2018
Published 15 August 2018
10.1126/scitranslmed.aap9527

Citation: W. D. Shipman, S. Chyou, A. Ramanathan, P. M. Izmirly, S. Sharma, T. Pannellini, D. C. Dasoveanu, X. Qing, C. M. Magro, R. D. Granstein, M. A. Lowes, E. G. Pamer, D. H. Kaplan, J. E. Salmon, B. J. Mehrara, J. W. Young, R. M. Clancy, C. P. Blobel, T. T. Lu, A protective Langerhans cell–keratinocyte axis that is dysfunctional in photosensitivity. *Sci. Transl. Med.* **10**, eaap9527 (2018).

Downloaded from http://stm.sciencemag.org/ by guest on August 20, 2018

Science Translational Medicine

A protective Langerhans cell–keratinocyte axis that is dysfunctional in photosensitivity

William D. Shipman, Susan Chyou, Anusha Ramanathan, Peter M. Izmirly, Sneh Sharma, Tania Pannellini, Dragos C. Dasoveanu, Xiaoping Qing, Cynthia M. Magro, Richard D. Granstein, Michelle A. Lowes, Eric G. Pamer, Daniel H. Kaplan, Jane E. Salmon, Babak J. Mehrara, James W. Young, Robert M. Clancy, Carl P. Blobel and Theresa T. Lu

Sci Transl Med **10**, eaap9527.
DOI: 10.1126/scitranslmed.aap9527

Abrogating keratinocyte apoptosis in lupus

Lupus patients can experience photosensitivity as manifested by joint pain, fatigue, and skin rashes. To better understand the mechanisms behind this photosensitivity, Shipman *et al.* examined patient skin samples and mouse models of lupus. They saw that, in healthy mice and human skin exposed to ultraviolet radiation, Langerhans cells protected keratinocytes from apoptosis through a mechanism involving the metalloproteinase ADAM17 and EGFR ligands. In the lupus mice and patient samples, the Langerhans cells were unable to do this. Stimulating EGFR in the skin may bring relief to photosensitive lupus patients.

ARTICLE TOOLS http://stm.sciencemag.org/content/10/454/eaap9527

SUPPLEMENTARY MATERIALS http://stm.sciencemag.org/content/suppl/2018/08/13/10.454.eaap9527.DC1

RELATED CONTENT
http://stm.sciencemag.org/content/scitransmed/10/434/eaan2306.full
http://stm.sciencemag.org/content/scitransmed/10/423/eaam8458.full
http://stm.sciencemag.org/content/scitransmed/10/450/eaam7710.full
http://stm.sciencemag.org/content/scitransmed/10/440/eaao4650.full

REFERENCES This article cites 50 articles, 19 of which you can access for free
http://stm.sciencemag.org/content/10/454/eaap9527#BIBL

PERMISSIONS http://www.sciencemag.org/help/reprints-and-permissions

Use of this article is subject to the Terms of Service

Science Translational Medicine (ISSN 1946-6242) is published by the American Association for the Advancement of Science, 1200 New York Avenue NW, Washington, DC 20005. 2017 © The Authors, some rights reserved; exclusive licensee American Association for the Advancement of Science. No claim to original U.S. Government Works. The title *Science Translational Medicine* is a registered trademark of AAAS.

Downloaded from http://stm.sciencemag.org/ by guest on August 20, 2018

Shipman et al. A protective Langerhans cell-keratinocyte axis that is dysfunctional in photosensitivity

SUPPLEMENTARY MATERIALS AND METHODS

Mice

Mice from 6-12 weeks old were used unless otherwise stated and were sex and aged-matched. Both male and female mice were used for experiments, except for B6.Sle1yaa mice, in which only males were used because the model is dependent in part on the autoimmune accelerator locus on the Y chromosome (*40*). C57BL/6J, Langerin-DTA, $Rag1^{-/-}$, Balb/c, MRL-MpJ, MRL-*Fas*^{lpr}, and B6.Sle1yaa mice were originally from Jackson Laboratory (JAX) and bred at our facility. CCR2-GFP and CCR2-DTR mice (*25*) were bred at our facility. $Rag1^{-/-}$ mice were intercrossed with Langerin-DTA mice to generate $Rag1^{-/-}$ Langerin-DTA mice. $ADAM17^{flox/flox}$ mice (*32*) were intercrossed with Langerin-$Cre^{+/-}$ mice (*33, 34*) (National Cancer Institute (NCI)), and Langerin-$Cre^{ER+/-}$YFP mice (*34*) to generate LC-Ad17 and Langerin-$Cre^{ER+/-}ADAM17^{flox/flox}$ mice, respectively. The WT mice used in experiments involving LC-Ad17 mice were Langerin-$Cre^{-/-}$ $ADAM17^{flox/flox}$ littermate controls. All animal procedures were performed in accordance with the regulations of the Institutional Animal Use and Care Committee at the Hospital for Special Surgery and Weill Cornell Medicine.

Human research participants

For immunofluorescence analysis, non-sun-exposed nonlesional skin from the buttocks of healthy controls and SLE patients was used. With the exception of one healthy control, all skin samples were from samples examined in (*53*). Controls were between the ages of 28-65 and 67% were female. The SLE patients met American College of Rheumatology criteria for SLE, were between the ages of 19-62 years old, and 79% were female. All SLE patients were

currently receiving treatment at the time of the biopsy (*53*). These samples were collected and used in accordance with the Institutional Review Board at the NYU School of Medicine (IRB# S14-00487).

For human LC and epidermal CD45+ non-LC cell isolation, human skin samples were collected from eleven human patients undergoing elective reconstructive surgery at the Division of Plastic and Reconstructive Surgery at the Memorial Sloan Kettering Cancer Center (MSKCC). Ten of the eleven patients were female and the patients were between the ages of 41-69 at the time of surgery. All tissue collection and research use adhered to protocols approved by the Institutional Review and Privacy Board at the Memorial Sloan Kettering Cancer Center, and all participants signed written informed consents (IRB# 06-107).

Mouse treatments

For indicated 24 hour experiments, HB-EGF (2ug; R&D Systems) dissolved in dimethyl sulfoxide (DMSO) was applied to each ear 15 minutes prior to UVR exposure. For long-term lesion development experiments, mice were shaved in a small area on the lower back. At 24 hours, HB-EGF was applied on the ears as above and on the shaved back area (8ug) for three consecutive days. Mice received their first dose of UVR on the last day of HB-EGF treatment.

Flow cytometry, cell sorting, and quantification

For staining of murine whole skin, single cell suspensions of skin were generated as previously described (*14*). Briefly, ear skin was excised, finely minced, digested in collagenase type II (616 U/mL; Worthington Biochemical Corporation), dispase (2.42 U/mL; Life Technologies),

and DNAse1 (80 μg/mL; Sigma-Aldrich), incubated at 37°C while shaking at 100 rpm, triturated with glass pipettes, and filtered. For murine epidermal cell staining or sorting, ear and trunk skin was incubated in dispase at 37°C for 45 minutes. The epidermis was then scraped off and finely minced before digestion in collagenase type II.

For flow cytometry analysis, the following gating strategies were used after excluding debris and non-single cells: *LCs:* Lineage(CD3, B220, NK, Ly6G)-, CD45+ CD11b+ CD24+, CD11c+, MHCII+; *monocytes*: Lineage-, CD45+, CD11b+, CD24-, Ly6C+, MHCII-; *monocyte-derived DCs*: Lineage- CD45+ CD11b+ CD24- $Ly6C^{hi-lo}$, MHCII+; *CD11b+ DCs*: Lineage- CD45+ CD24- CD11b+ Ly6C- CD64- CD11c+ MHCII+; *CD11b- DCs*: Lineage- CD45+ CD11b- CD24+ CD11c+ MHCII+; *macrophages:* Lineage- CD45+ CD11b+ CD24- CD64+; *neutrophils:* Lineage+ CD11b+ $Ly6C^{med}$, side scatter $(SSC)^{hi}$; *T cells*: epidermal CD45+, CD11b-, CD3+; *keratinocytes*: epidermal CD45-, CD31-, EpCAM+ or total skin CD45-, CD31-, CD49f+, Sca1+, EpCAM+; *skin plasma cells*: CD45+, $B220^{lo}$, CD3-, intracellular IgG^{hi}; *lymph node germinal center B cells*: CD3-, B220+, PNA+; *lymph node plasma cells:* CD3-, $B220^{lo}$, CD138+. LCs, monocytes, monocyte-derived DCs, CD11b+ DCs, CD11b- DCs, and macrophages were gated according to Tamoutounour et al. (*24*). Primary and secondary antibodies are described in Table S1 and Table S2.

For flow cytometry analysis, cells were analyzed using a FACSCanto (BD Biosciences) and FlowJo Software (Tree Star). Cells were sorted using a BD Influx.

To measure phosphoEGFR by flow cytometry, cells were serum- or EGF-starved, pretreated with 2 mM $NaVO_3$ for 15 minutes, fixed with 4% paraformaldehyde for 15 minutes at room temperature, and then permeabilized with ice-cold methanol (90%) for 30 minutes on ice. The cells were then stained with anti-phosphoEGFR Tyr1068 (Cell Signaling) followed by anti-rabbit Alexa647 (Jackson Immunoresearch).

For isolation of murine epidermal cells for cultures and qPCR, epidermal single cell suspensions from ear and back skin were flow sorted for CD45+CD11b+ EpCAM+ CD3- LCs, CD45+CD3+CD11b- T cells, and CD45-, CD31-, EpCAM+ keratinocytes. Purity of sorted cells was >95%.

For human LC and CD45+ non-LC isolations, fresh skin samples were obtained from patients undergoing elective reconstructive surgery as described above. Skin samples were cut into small pieces and incubated for 30 min at 37°C and 5% CO_2 in prewarmed DMEM/F-12 (Stem Cell Technologies) with dispase II (1 IU/ml; Roche Diagnostics) to facilitate separation of the epidermis from the dermis. The epidermis was gently peeled away from the dermis and placed in RPMI 1640 supplemented with 10 mM HEPES, 1% penicillin/streptomycin (Media Lab, MSKCC), 50 mM L-glutamine (Cellgro), 50 μM β-mercaptoethanol (Gibco, Life Technologies), and 10% heat-inactivated pooled healthy human serum (Atlanta Biologicals). The epidermal sheets were then finely minced and digested with collagenase as described for mouse epidermis. LCs (CD45+ CD1a+ HLADR+), non-LC CD45+ cells (CD45+ CD1a- HLADR-), T cells (CD45+ CD1a- HLADR- CD3+), and keratinocytes (CD45- CD1a- CD3- EpCAM+) were sorted and sorted cells had a purity ≥ 95%.

Human epidermal cells used for flow cytometric analysis of ADAM17 were incubated with human TruStain FcX Fc receptor blocking solution (BioLegend), the cells were then stained with anti-human ADAM17 (Abcam) or human IgG1 isotype control (Adipogen), followed by anti-human IgG biotin (Jackson Immunoresearch) and streptavidin Alexa 488 (Thermo Fisher Scientific- Invitrogen). After excluding debris, dead cells, and non-single cells the following gating strategies were used to examine ADAM17 expression: LCs: CD45+ CD1a+ HLADR+ CD3-, T cells: CD45+ CD3+ CD1a- HLADR- and keratinocytes: CD45- CD1a- HLADR- EpCAM+.

Cells were counted using a Z1 Coulter Counter (Beckman Coulter). To calculate absolute cell numbers, the percentage of the total of a particular population was multiplied by the total cell count from the Coulter Counter. For figures showing normalized values, the control sample was set to 1, and the experimental samples were normalized relative to the control for that experiment. For experiments that contained more than one control sample, the mean was obtained for the control samples, and the individual control and experimental samples were calculated relative to this mean.

Histology, immunofluorescence staining, and quantifications

For immunofluorescence staining of murine skin, frozen unfixed mouse skin was sectioned, fixed with cold acetone for 10 minutes, and stained as indicated (*15*). Epidermal activated caspase-3+ cells per high powered field (40x magnification) were quantified by a blinded observer using ImageJ software (NIH) and classified as activated caspase-3+ keratinocytes (Langerin- and CD3-), LCs (Langerin+), or T cells (CD3+).

Formalin-fixed paraffin embedded murine skin was stained with hematoxylin and eosin, and epidermal thickness was measured by a blinded observer using ImageJ software.

For immunofluorescence staining of cell culture experiments, polystyrene chamberslides (Lab-Tek) with cultured keratinocytes were washed with PBS, fixed with 4% paraformaldehyde for 20 minutes, permeabilized and blocked with Triton-X (0.2%) and BSA (1%), and stained as indicated. Activated caspase-3+ and total DAPI+ cells were quantified with ImageJ software by a blinded observer and the percent of activated caspase-3+ Langerin- cells (keratinocytes) and activated caspase-3+ Langerin+ cells (LCs) was calculated.

For immunofluorescence staining of human skin, formalin-fixed paraffin-embedded tissue sections were rehydrated and underwent antigen retrieval at 60°C in 10 mM citrate buffer, pH

6.0 for 20 hours followed by enzymatic retrieval with Carezyme III: Pronase Kit (Biocare Medical) for 15 minutes. Sections were then stained as indicated. The fluorescence intensity of phosphoEGFR and total EGFR was measured using ImageJ software and the fluorescence intensity of the isotype control was subtracted. The ratio of phosphoEGFR:total EGFR was then calculated and normalized to the ratio for the healthy control samples that were stained at the same time as the SLE samples. Langerin+ cells in the epidermis were counted by a blinded observer using ImageJ software and normalized to the length of the tissue.

All antibodies and staining reagents are described in Table S1 and Table S2. Histology was imaged using either a Nikon Eclipse E600 with a Q-Imaging Retiga Exi camera or a Nikon Eclipse NI-E Fluorescence Upright microscope coupled to a Zyla sCMOS camera (Andor Technology).

Western blots

Western blots were performed essentially as described (*23*). Ears were harvested and the epidermis was isolated by incubating skin in distilled water at 60 °C for 20 seconds and then in ice cold PBS for 20 seconds before the epidermis was gently scraped off. Epidermal sheets were then lysed on ice with a Polytron PT 10-35 tissue homogenizer in lysis buffer (50 mM Tris-HCl pH 7.7, 1% Triton-X, 150 mM NaCl, 1 mM EDTA, 10 mM NaF, 5 mM β-glycerophosphate, 2 mM $NaVO_3$, 1 mM 1,10-ortho-phenanthroline (Sigma-Aldrich), and protease inhibitor cocktail set III (EMD Millipore)). Samples (10-15 µg protein) were separated on a 10% SDS-polyacrylamide gel, transferred to nitrocellulose paper, and Western blots were then stained as indicated. Antibody staining was detected using ECL Plus Western blotting substrate (Thermo Fisher Scientific). Blots were first stained for phosphoEGFR, stripped with 1 M Tris pH 6.75, β-mercaptoethanol, and SDS at room temperature followed by incubation at 60

°C, and then reprobed for total EGFR. All antibodies used for Western blots are described in Table S1 and Table S2. Western blots were quantified with ImageJ software and the ratio of phosphoEGFR: total EGFR was determined and normalized to the ratio of the control samples.

Epidermal permeability measurement

Toluidine blue dye penetrance was measured essentially as described (*23*). Dehydrated and rehydrated ear skin was incubated for 2 min in 0.1% toluidine blue dye (Sigma-Aldrich) before destaining and toluidine blue dye extraction with a solution of 2.5% H_2SO_4, 2.5% H_2O, and 95% methanol. Colorimetric values were measured at 620 nm and the total amount of toluidine blue dye was calculated using the volume of extraction solution, which was constant among the conditions.

In vitro experiments

Mouse keratinocyte-LC co-cultures:

Primary mouse keratinocyte cultures were prepared from mouse tail skin as described (*23*). The isolated epidermal cells were plated in 8-well chamberslides (Lab-Tek) coated with 7 ng/μL collagen I (BD Biosciences) at 2-4 x 10^5 cells per well in serum-free keratinocyte growth media 2 (KGM2) (PromoCell). 3-4 days later, keratinocytes were at 90% confluency and sorted LCs were added at a density of 20,000-25,000 LCs per well. The co-cultures rested overnight and were then exposed to UVR and analyzed 24 hours later. Unless indicated, co-cultures were exposed to UVR in approximately 200 μL of minimally colored culture media containing 3.3 mM phenol red and without a plastic covering.

Keratinocyte EGFR knockdown co-cultures:

Primary mouse keratinocytes were cultured as described above and, at 40-50% confluency, were treated with control siRNA or two different EGFR siRNAs (siRNA #1 or #2) (Accell siRNA from Dharmacon, GE Lifesciences) according to the manufacturer's protocol. Target sequences of the siRNAs were: siRNA #1- 5'-GAUUGGUGCUGUGCGAUUC-3' and siRNA #2- 5'-GCAUAGGCAUUGGUGAAUU-3'. The media was changed to normal keratinocyte growth media on day 4, and the co-culture experiments were subsequently conducted as described in Materials and Methods in the main text. Separate wells on the same chamberslides were collected on day 5 (the day of UVR exposure) to check efficiency of EGFR knockdown by flow cytometry.

Keratinocyte PD168393 treatment co-cultures:

Primary mouse keratinocytes were treated with 2 μM PD168393 (Cayman Chemicals), an irreversible EGFR inhibitor, for 30 minutes. The PD168393 was washed off with PBS and fresh keratinocyte growth media was supplied with or without LCs and the co-culture experiments were subsequently conducted. Keratinocytes from separate wells were collected at the time of co-culture and treated with EGF (200 ng/mL) to validate the efficiency of EGFR inhibition by measuring phosphoEGFR by flow cytometry.

Human keratinocyte-LC co-cultures:

Primary human keratinocytes (Lonza) were prepared according to the manufacturer's protocol and plated on collagen-coated chamberslides at 1-2 days before use. Human LCs and non-LC CD45+ cells were sorted from epidermis and added to 50-90% confluent keratinocyte cultures at 16,000-20,000 cells per chamberslide well. The co-cultures were rested overnight, exposed

to UVR, and examined 24 hours after UVR. Some wells of keratinocytes were treated with recombinant human HB-EGF (R&D Systems) at indicated concentrations, rested overnight, and then exposed to UVR. For anti-ADAM17 blocking experiments, LCs were pretreated with 200 nM of anti-human ADAM17 blocking antibody (Abcam) or human IgG1 isotype control antibody (Adipogen) for 30 minutes before they were added with the antibodies to the keratinocytes. Anti-ADAM17 blocking antibody and IgG1 isotype control antibody was also included in keratinocyte cultures without LCs as additional controls.

Ex vivo ADAM17 activity assay by TNFR1 cleavage

Sorted mouse LCs were plated in a 96-well plate at 20,000-25,000 cells/well in RPMI 1640 supplemented with L-glutamine, penicillin/streptomycin, and HEPES buffer. The cells were treated with phorbol 12-myristate 13-acetate (PMA) (Sigma-Aldrich) at 25 ng/mL or UVR (500 J/m^2) and analyzed 45 minutes later. The cells were then stained with DAPI to exclude dead cells and for cell-surface TNFR1 (BioLegend). ADAM17 activity is expressed as the percent change in TNFR1 mean fluorescence intensity (MFI) relative to that of untreated LCs. Sorted human LCs (3,000-5,000 cells/well) were plated and treated with anti-ADAM17 blocking antibody or human IgG1 isotype control antibody for 30 minutes prior to UVR exposure and analysis of TNFR1 MFI. For collection of conditioned supernatant from sorted human LCs to add to A431 cells, 1,500 LCs were treated with IgG control or anti-ADAM17 blocking antibody for 30 minutes, washed, and then transferred into new media prior to UVR treatment to prevent carryover of blocking antibodies into the conditioned supernatant.

EGFR ligand release assay with A431 indicator cells

A431 human squamous carcinoma cells (ATCC) were cultured according to the manufacturer's protocol in 96 well plates. At about 80% confluency, the A431 cells were serum-starved overnight then pretreated with 2 mM $NaVO_3$ for 15 minutes at 37° C, and were then treated with conditioned supernatants from various cells for 10 minutes. The A431 cells were then collected and phosphoEGFR expression was measured by flow cytometry. All experiments were conducted with A431 cells in passage 2.

Lesion quantification

The remaining hair on the back skin of the mice was removed using Nair and photographs were taken. The total back area and lesional area (skin affected by erythema, scaliness, crustiness, or epidermal erosion) was measured by a blinded observer using ImageJ software and skin lesions were quantified as percent of back area.

mRNA quantification

Cells were sorted directly into RLT lysis buffer (Qiagen) with β-mercaptoethanol (Bio-Rad) and stored at -80°C until RNA extraction with Qiagen RNeasy Mini Kit. cDNA was generated using iScript cDNA synthesis kit (Bio-Rad) and real-time PCR was performed using iQ SYBR Green Supermix kit (Bio-Rad) on a Bio-Rad MyiQ thermal cycler or Maxima SYBR Green/ROX qPCR Master Mix (Thermo Fisher Scientific) on a StepOne Plus Real-Time PCR system (Applied Biosystems). qPCR gene expression was quantified relative to *Gapdh*. Primer sequences used were:

Mouse (5'-3'):

Epgn forward: TGGGGGTTCTGATAGCAGTC, *Epgn* reverse: GGATCACCTCTGCTTCTTCG, *Egf* forward: CCTGGGAATGTGATTGCTTT, *Egf* reverse: CCTGGGAATTTGCAAACAGT, *Hbegf* forward: CCACCTCACTCCCTTTGTGT, *Hbegf* reverse: AAAGCTCCCTGCTCTTCCTC, *Tgfa* forward: AAGGCATCTTGGGACAACAC, *Tgfa* reverse: GCAGGCAGCTTTATCACACA, *Btc* forward: GGGTGTTTCCCTGCTCTGTA, *Btc* reverse: TGGATGAGTCCTCAGGTTCC, *Areg* forward: CATTATGCAGCTGCTTTGGA, *Areg* reverse: TTTCGCTTATGGTGGAAACC, *Ereg* forward: CGCTGCTTTGTCTAGGTTCC, *Ereg* reverse: GGGATCGTCTTCCATCTGAA, *Adam17* forward: GATGCTGAAGATGACACTGTG, *Adam17* reverse: GAGTTGTCAGTGTCAACGC, *Gapdh* forward: ATGTGTCCGTCGTGGATCTGA, *Gapdh* reverse: TTGAAGTCGCAGGAGACAACCT.

Human (5’-3’):

Epgn forward: ATGACAGCACTGACCGAAGAG, *Epgn* reverse: AACTGTCCAGTTACCTTGCTG, *Egf* forward: TCTCAACCCCTTGTACTTTGG, *Egf* reverse: CAAGTCATCCTCCCATCACCA, *Hbegf* forward: TTGTGCTCAAGGAATCGGCT, *Hbegf* reverse: CAACTGGGGACGAAGGAGTC, *Tgfa* forward: TCGTGAGCCCTCGGTAAGTA, *Tgfa* reverse: GACTGGTCCCCCTTTCATGG, *Btc* forward: AAAGCGGAAAGGCCACTTCT, *Btc* reverse: AGCCTTCATCACAGACACAGG, *Areg* forward: TGTCGCTCTTGATATCGGC, A*reg* reverse: ATGGTTCACGCTTCCCAGAG, *Ereg* forward: TACTGCAGGTGTGAAGTGGG, *Ereg* reverse: GTGGAACCGACGACTGTGAT, *Adam17* forward: TGATGAGCCAGCCAGGAGAT, *Adam17* reverse: TATCAAGTCTTGTGGGGACAGC, *Gapdh* forward: CGACAGTCAGCCGCATCTT, *Gapdh* reverse: ATCCGTTGACTCCGACCTTC.

Skin histopathology scoring

A blinded expert dermatopathologist scored H&E stained sections based on dermal inflammation (0-3).

SUPPLEMENTARY FIGURES

Fig. S1

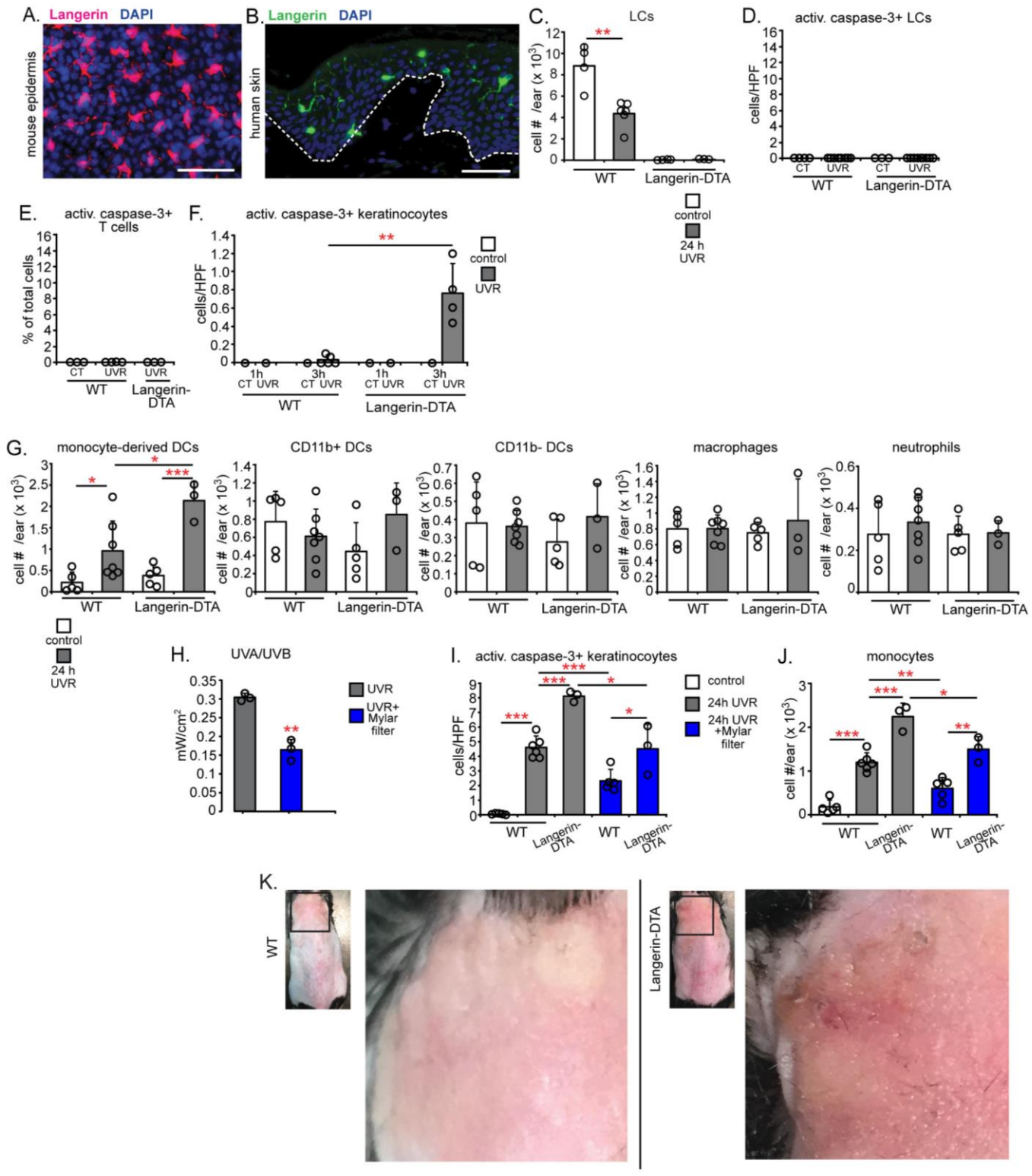

Fig. S1. Additional features of LC-mediated protection from UVR-induced keratinocyte apoptosis and skin injury. (A) Representative image of mouse epidermal whole mount

stained with anti-Langerin (pink) and DAPI (blue) (n= 3 mice). **(B)** Representative image of human skin stained with anti-Langerin (green) and DAPI (blue) (n= 3 healthy control human patients). Dashed line indicates epidermal-dermal junction. **(A,B)** Scale bar: 50 μm. **(C-E)** WT and Langerin-DTA mice were treated with UVR and ears examined at 24 hours as in Fig. 1A-C. **(C)** LC numbers as assessed by flow cytometry (n= 3-6 mice). **(D)** Activated caspase-3+ Langerin+ LC numbers in tissue sections (n= 3-9 mice). **(E)** Activated caspase-3+ CD3+ T cell numbers (n= 3-4 mice). **(F)** Activated caspase-3+ keratinocyte numbers at indicated time after UVR exposure (n= 1-4 mice). **(G)** Absolute numbers of monocyte-derived DCs, CD11b+ DCs, CD11b- DCs, macrophages, and neutrophils at 24 hours after UVR exposure (n= 3-7 mice). **(H)** UVA/UVB measurements of UVR source without and with Mylar filter (n= 3). Each symbol represents the value measured during independent experiments. **(I,J)** WT and Langerin-DTA mice were treated with UVR or UVR+Mylar filter and examined with non-exposed controls at 24 hours (n= 3-6 mice). **(I)** Activated caspase-3+ keratinocyte numbers. **(J)** Absolute monocyte numbers. **(K)** Magnified images of back skin from UVR-exposed WT and Langerin-DTA mice described in Fig. 1G,H (n= 3-5 mice). **(C-G,I-K)** Each symbol represents 1 mouse**.** Data from 3 **(A,B,E,H-K)**, 5 **(C)**, 9 **(D),** 2 **(F),** and 7 **(G)** independent experiments. Bars represent means and error bars depict standard deviations. *****$p<0.05$, **$p<0.01$, ***$p<0.001$ using two-tailed unpaired Student's t-test. T-test was performed after one-way ANOVA for **(C-G, I, J)**.

Fig. S2

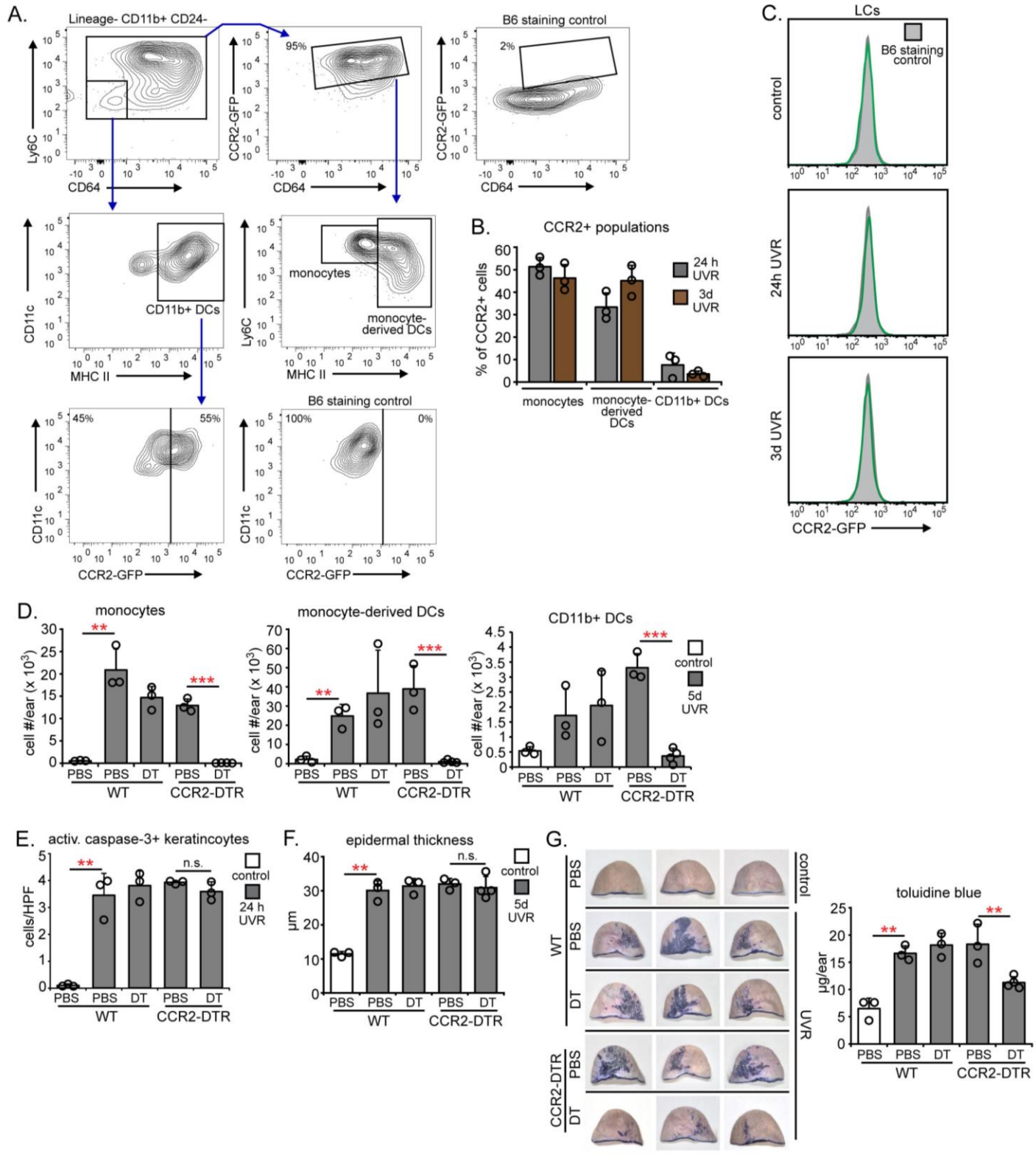

Fig. S2. The role of accumulated monocytes and monocyte-derived DCs in UVR-induced skin injury. **(A-C)** CCR2-GFP reporter mice were exposed to UVR and ears were examined at

indicated time points along with a B6 staining control (n= 3 mice). **(A)** Flow cytometry gating strategy for CCR2+ populations in the skin using the scheme of Tamoutounour et. al (*24*). Lineage= B220, CD3, Ly6G, and pan-NK CD49b **(B)** Percentage of CCR2+ cells in the skin that are monocytes, monocyte-derived DCs, and CD11b+ DCs. **(C)** Representative histograms of CCR2-GFP expression in LCs as assessed by flow cytometry (n= 3 mice). **(D-G)** WT and CCR2-DTR mice were injected with PBS or 250 ng DT at d-1 and d0 of UVR exposure and examined 24 hours later with non-exposed control mice (n= 3 mice) **(E),** or injected with PBS or DT at d-1, d0, and d3 of UVR exposure and examined 5 days later with non-exposed control mice (n= 3-4 mice) **(D,F,G)**. **(D)** Monocyte, monocyte-derived DC, and CD11b+ DC depletion at 5 days after UVR exposure. **(E)** Activated caspase-3+ keratinocyte numbers. **(F)** Epidermal thickness. **(G)** Epidermal permeability. Left: Representative images of toluidine blue penetrance. Right: Quantification. **(B,D-G)** Each symbol represents 1 mouse**.** Data from 2 **(A-C,E)** and 3 **(D,F,G)** independent experiments. Bars represent means and error bars depict standard deviations. n.s.= not significant $p \geq 0.05$,**$p<0.01$, ***$p<0.001$ using two-tailed unpaired Student's t-test after one-way ANOVA.

Fig. S3

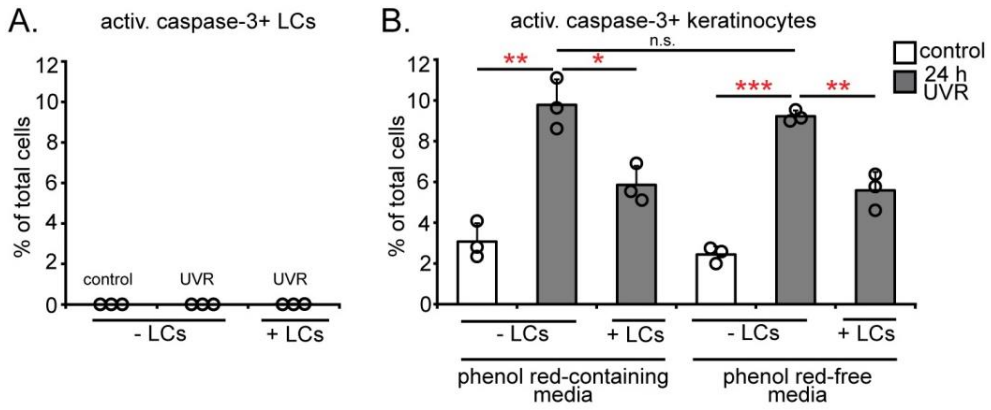

Fig. S3. Additional features of LC-mediated protection of keratinocytes in vitro. (A) Murine keratinocyte cultures without and with LCs were exposed to UVR (as in Fig. 2D,E) and activated caspase-3+ cells that were Langerin+ (LCs) were quantified (n= 3 mice). **(B)** LC-mediated protection of keratinocytes in the absence of phenol red. Murine keratinocyte cultures without and with LCs were exposed to UVR in phenol red-containing media (used for most experiments) or phenol red-free keratinocyte growth media and activated caspase-3+ keratinocyte numbers were quantified (n= 3 mice). Results are from 3 **(A)** and 2 **(B)** independent experiments, with each symbol representing a biological replicate. Each biological replicate value is the mean obtained from 2-6 replicate wells. n.s.= not significant $p \geq 0.05$, ***p<0.05, **p<0.01, ***p<0.001 using two-tailed unpaired Student's t-test after one-way ANOVA.

Fig. S4

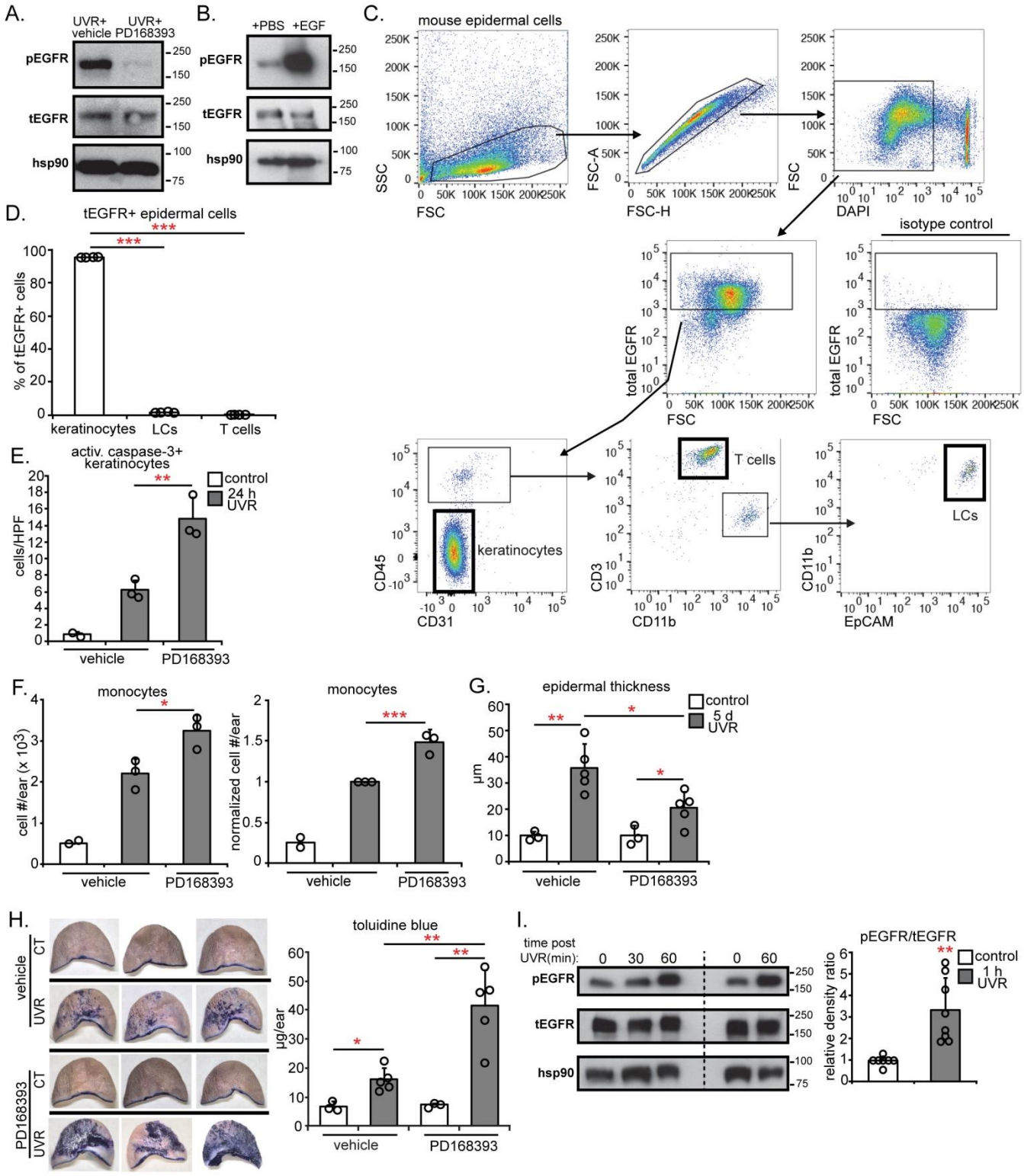

Fig. S4. Mice treated with EGFR inhibitor resemble Langerin-DTA mice and timing of epidermal EGFR activation after UVR exposure. (A, E-H) Mice were treated topically with 4mM EGFR inhibitor-PD168393 or vehicle prior to UVR exposure and examined at indicated

time points. **(A)** Representative Western blot of epidermal EGFR phosphorylation at 1 hour after UVR (n= 3 mice). **(B)** Positive control for EGFR phosphorylation, showing effects of intradermally injected recombinant EGF (5µg) at 5 minutes (n= 2 mice). **(C)** Flow cytometry gating strategy for total EGFR (tEGFR)+ cells in the epidermis. **(D)** Percent of tEGFR+ cells in each epidermal cell population examined (n= 4 mice). **(E)** Activated caspase-3+ keratinocyte numbers (n= 2-3 mice). **(F)** Absolute (left) and normalized (right) monocyte numbers (n= 2-3 mice) **(G)** Epidermal thickness (n= 3-5 mice). **(H)** Epidermal permeability. Representative images of toluidine blue-treated ears (left) and quantification (right) (n= 3-5 mice). **(I)** Left: Representative Western blot at the indicated time points after UVR exposure. Right: phosphoEGFR:total EGFR relative density ratio (n= 7-8 mice). **(D-I)** Each symbol represents 1 mouse**.** Data from 3 **(A,E,F)**, 1 **(B,D)**, 2 **(G,H)**, and 4 **(I)** independent experiments. Bars represent means and error bars depict standard deviations. *****p<0.05, **p<0.01, ***p<0.001 using two-tailed unpaired Student's t-test. T-test was performed after one-way ANOVA for **(D-H)**.

Fig. S5

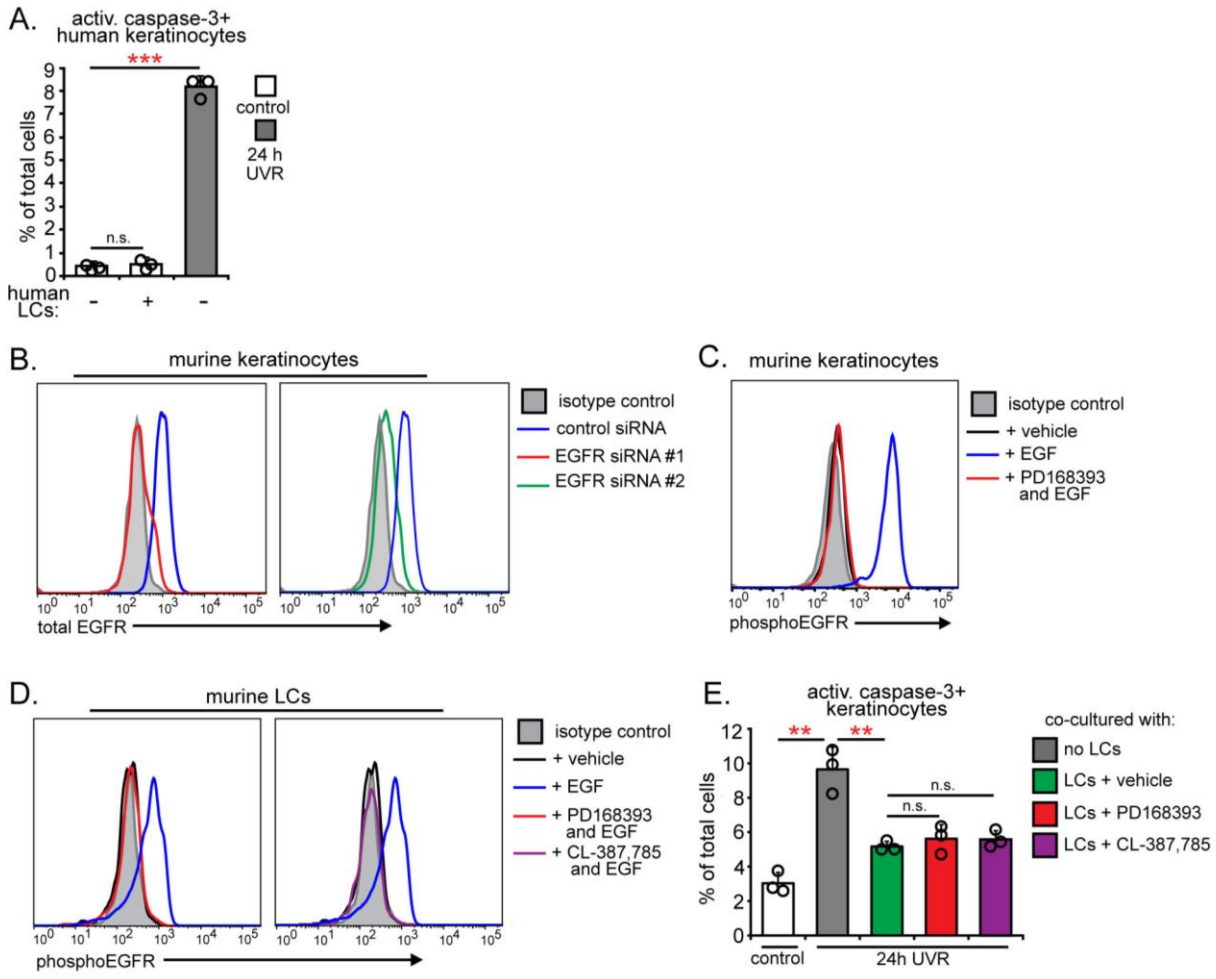

Fig. S5. Effect of human LCs on human keratinocytes without UVR and further characterization of in vitro LC-keratinocyte EGFR signaling (A) Effect of human LCs on human keratinocytes without UVR. Primary human keratinocytes were co-cultured with or without human LCs and activated caspase-3+ keratinocytes were enumerated 24 hours later (n= 3 human LC donors). **(B)** Validation of siRNA-mediated EGFR knockdown in primary murine keratinocytes. Keratinocytes were treated with control or EGFR-targeted siRNAs (#1 and #2) and EGFR expression was measured 5 days later (on the day of UVR exposure as in Fig. 3F) by flow cytometry. Representative histogram of EGFR expression in keratinocytes. (n= 4 mice). **(C)** Validation of pharmacological EGFR inhibition in primary murine keratinocytes.

EGF-starved primary murine keratinocytes were pre-treated with vehicle or 2 μM PD168393 for 30 minutes, then treated with EGF (200 ng/mL) for 10 minutes, and phosphoEGFR was then measured by flow cytometry. Representative histogram of phosphoEGFR expression in keratinocytes (n= 3 mice). **(D)** Validation of pharmacological EGFR inhibition in LCs. LCs were sorted from WT mice, serum-starved, pre-treated with vehicle, 2 μM PD168393, or an alternate EGFR inhibitor, CL-387,785 (1 μM) for 30 minutes, then treated with EGF (200 ng/mL) for 10 minutes, and phosphoEGFR measured by flow cytometry. Representative histogram of phosphoEGFR expression in LCs (n= 3 mice). **(E)** Effect of LC EGFR inhibition on LC-mediated protection of keratinocytes. Murine keratinocyte cultures without and with the indicated pre-treated LCs were exposed to UVR and activated caspase-3+ keratinocytes were enumerated 24 hours later (n= 3 mice). Results are from 4 **(B)**, 2 **(C,E)**, and 3 **(A,D)** independent experiments. **(A,D)** Each symbol represents a biological replicate and each biological replicate value is the mean obtained from 2-3 replicate wells. Bars represent means and error bars depict standard deviations. n.s.= not significant $p \geq 0.05$, $^{**}p < 0.01$ using two-tailed unpaired Student's t-test after one-way ANOVA.

Fig. S6

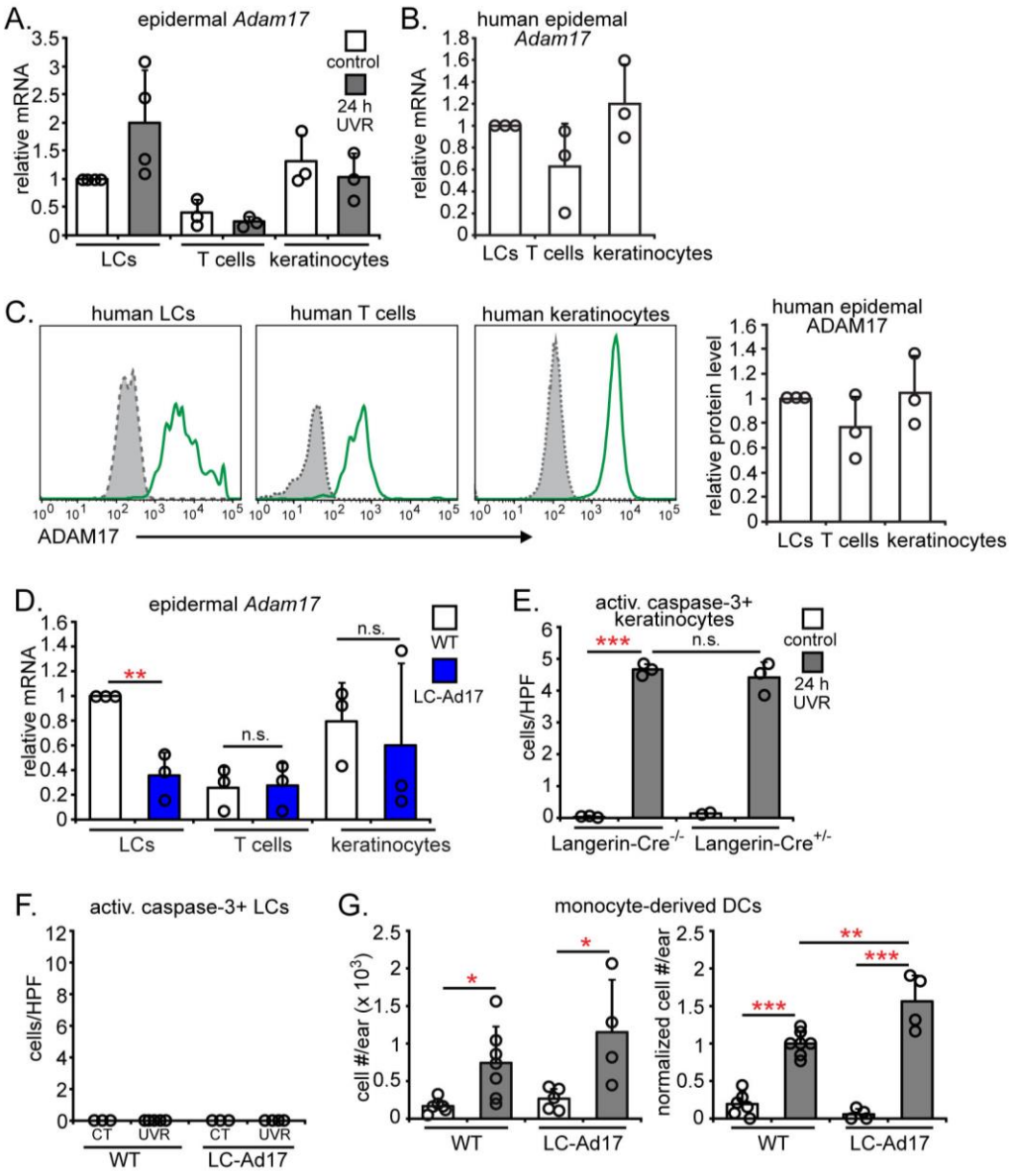

Fig. S6. Characterization of mouse and human ADAM17 expression, LC-Ad17 mice, and Langerin-Cre mice (A) *Adam17* expression in epidermal cell subsets sorted from non-exposed WT mice or from mice at 24 hours after UVR exposure, normalized to control LC expression (n= 3-4 mice). **(B)** *Adam17* mRNA expression in sorted LCs, T cells, and keratinocytes from healthy human skin, normalized to LC expression (n= 3 human donors). **(C)** ADAM17 cell surface protein expression on human LCs, T cells, and keratinocytes as assessed by flow cytometry (n= 3 human donors). Top: Representative histograms. Bottom:

Quantification of relative ADAM17 protein levels. MFI of ADAM17 stain was first divided by MFI of isotype control to quantify fold-over-isotype for each cell type and the fold-over-isotype for each cell type was then expressed relative to that of LC ADAM17. **(D)** *Adam17* expression in epidermal cell subsets sorted from WT and LC-Ad17 mice at homeostasis normalized to WT LC expression (n= 3 mice). **(E)** Langerin-Cre$^{-/-}$ and Langerin-Cre$^{+/-}$ mice were exposed to UVR and activated caspase-3+ keratinocytes quantified (n= 2-3 mice). **(F)** Activated caspase-3+ LC numbers in WT and LC-Ad17 mice (n= 3-5 mice). Data are from same mice as in Fig. 5A. **(G)** Absolute (left) and normalized (right) monocyte-derived DC numbers in WT and LC-Ad17 mice (n= 4-7 mice). **(A-G)** Each symbol represents 1 mouse or 1 human donor. Data from 4 **(A)**, 3 **(B-F)**, or 5 **(G)** independent experiments. Bars represent means and error bars depict standard deviations. n.s.= not significant $p \geq 0.05$, *****$p<0.05$, **$p<0.01$, ***$p<0.001$ using two-tailed unpaired Student's t-test after one-way ANOVA.

Fig. S7

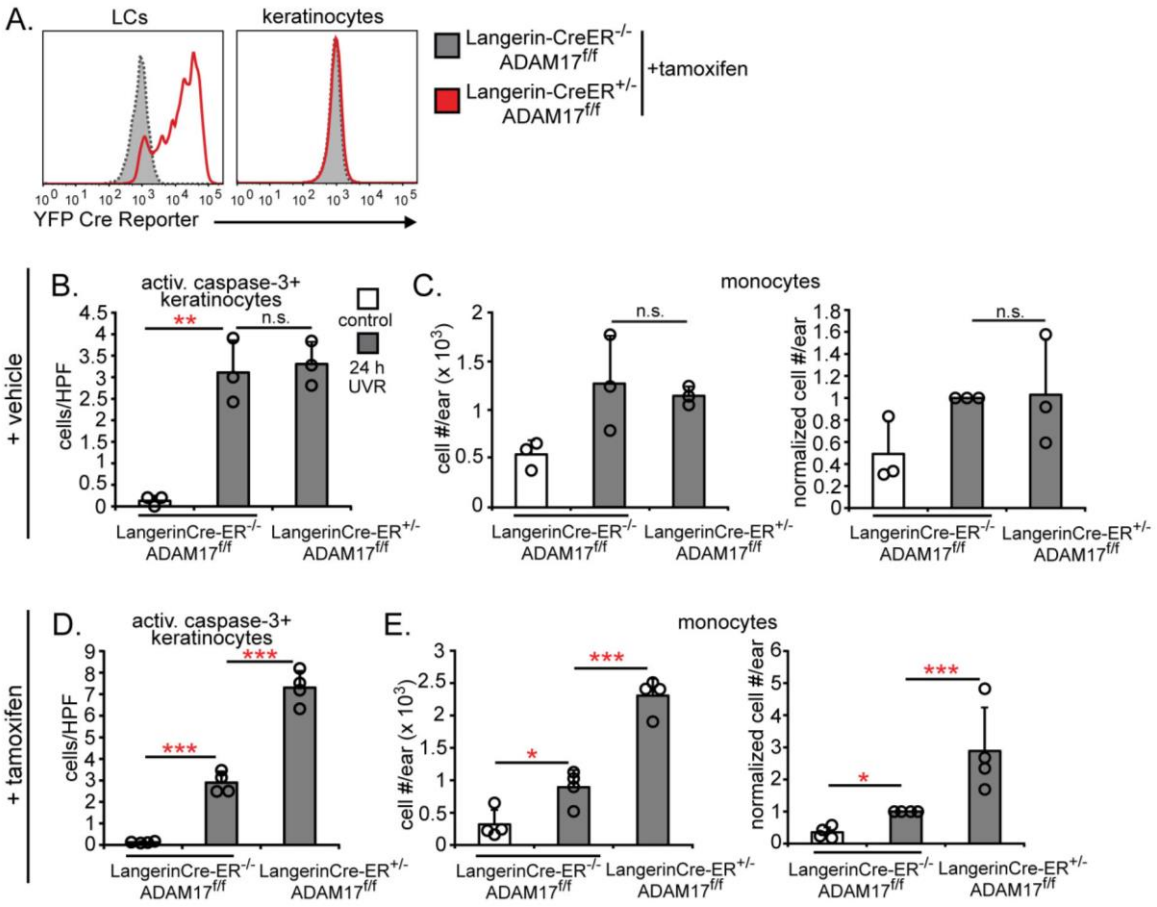

Fig. S7. Effects of inducible ADAM17 deletion in LCs. (A-E) Langerin-Cre-ER$^{-/-}$ ADAM17$^{flox/flox}$ and Langerin-Cre-ER$^{+/-}$ADAM17$^{flox/flox}$ mice containing a Rosa26.STOP^{fl}.YFP Cre reporter allele were generated and treated topically with vehicle (n= 3 mice) **(B,C)** or 1 ng/mL 4-hydroxytamoxifen (n= 4 mice) **(A,D,E)**. Six days later, they were either examined **(A)** or exposed to UVR and analyzed at 24 hours **(B-E).** **(A)** Cre expression in LCs. Shown is representative histogram of YFP levels in LCs and keratinocytes. **(B,D)** Activated caspase-3+ keratinocyte numbers. **(C,E)** Absolute (left) and normalized (right) monocyte numbers. **(B-E)** Each symbol represents 1 mouse. Data from 2 (A,D,E) and 1 (B,C) independent experiments. Bars represent means and error bars depict standard deviations. n.s.= not significant $p \geq 0.05$, ***p<0.05, **p<0.01, ***p<0.001 using two-tailed unpaired Student's t-test after one-way ANOVA.

Fig. S8

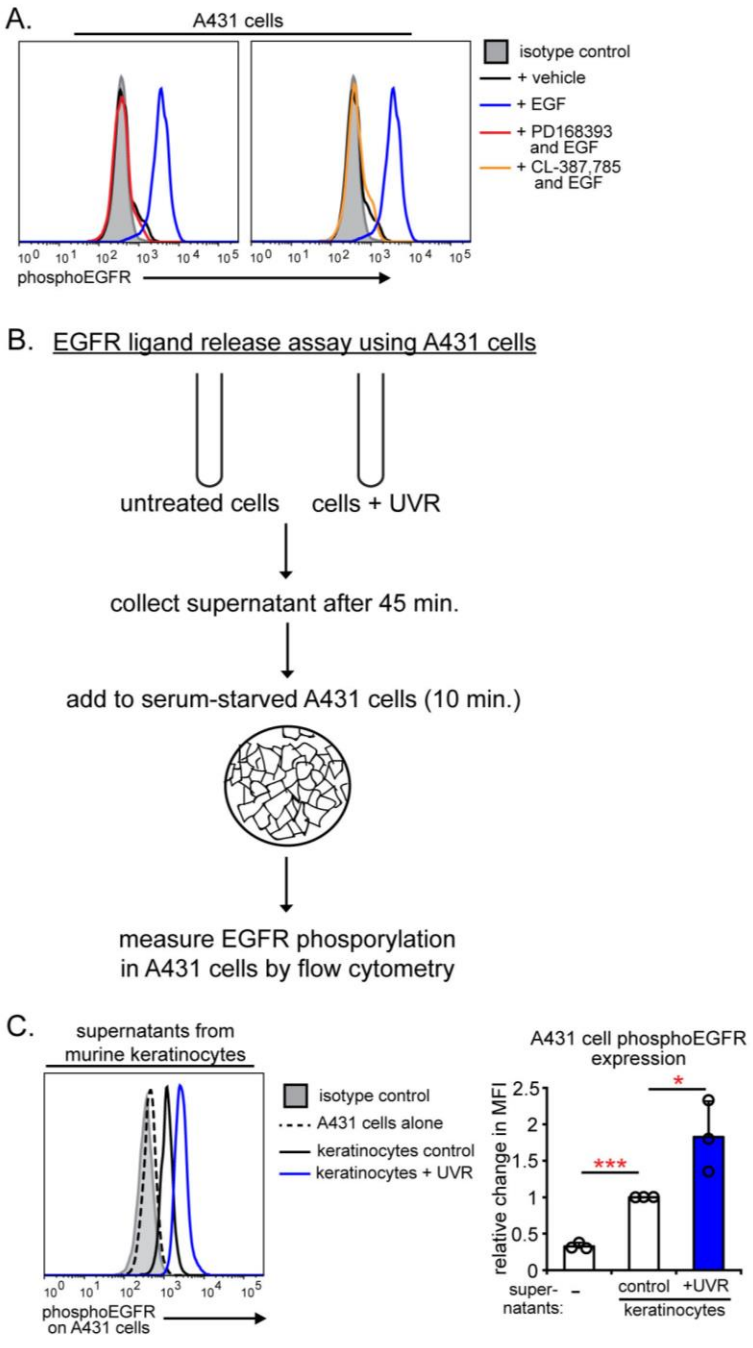

Fig. S8. Validation of EGFR ligand release assay and characterization of keratinocyte EGFR ligand release. (A) A431 indicator cells were serum-starved overnight then pre-treated for 15 minutes with vehicle, the irreversible EGFR inhibitors PD168393 (2 μM), or CL-387,785 (1 μM). The cells were then treated with EGF (100 ng/mL) for 10 minutes and phosphoEGFR

was measured by flow cytometry (n= 2 separate cell passages). **(B)** Schematic diagram of EGFR ligand release assay using A431 indicator cells. Cells (sorted murine LCs, sorted human LCs, or primary murine keratinocytes) were treated or not with UVR and the conditioned supernatant was collected and added to serum-starved A431 cells for 10 minutes. The A431 cells were then collected and phosphoEGFR was measured by flow cytometry as an indicator of the level of EGFR ligand in the conditioned supernatant. **(C)** Characterization of murine primary keratinocyte EGFR ligand release. Confluent primary murine keratinocytes were exposed to UVR and the supernatant of these cells and non-exposed control keratinocytes was collected 45 minutes later and added to A431 cells as described in Fig. S7B. Left: Representative histogram of phosphoEGFR expression in the A431 cells. Right: Quantification of A431 cell phosphoEGFR expression normalized to the expression with control keratinocyte supernatants (n= 3 mice). Results are from 2 **(A,C)** independent experiments. **(C)** Each symbol represents a biological replicate. Bars represent means and error bars depict standard deviations. ***$p<0.001$, *$p<0.05$ using two-tailed unpaired Student's t-test after one-way ANOVA.

Fig. S9

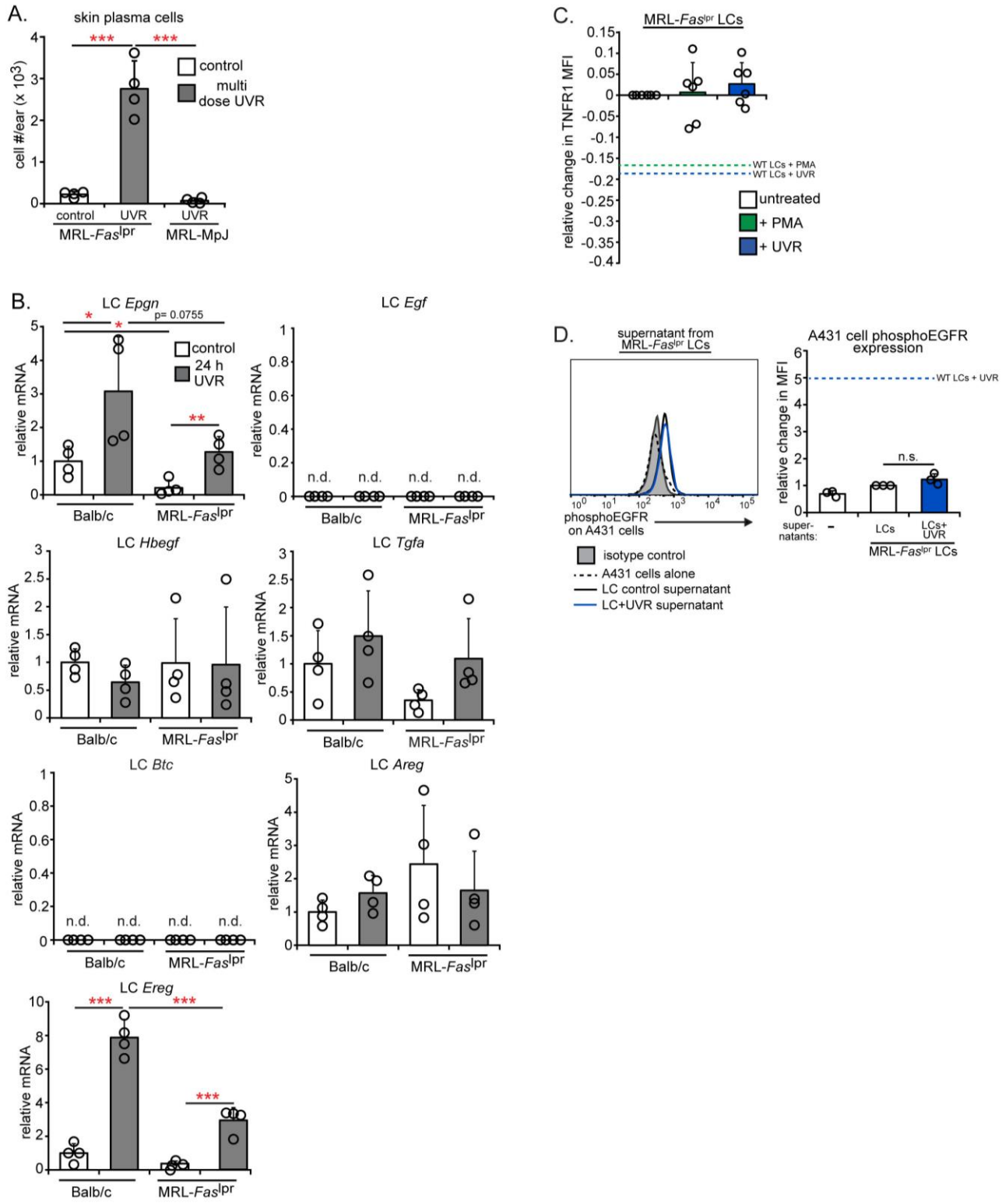

Fig. S9. Photosensitive MRL-*Fas*^{lpr} mice have more skin plasma cells and reduced LC EGFR ligand expression, LC ADAM17 activity, and LC EGFR ligand release. (A,B) MRL-

Fas^{lpr} and non-lupus MRL-MpJ or Balb/c mice were exposed to UVR as indicated and skin from these and non-exposed control mice were examined 24 hours after the final exposure (n= 4 mice). **(A)** Skin plasma cells (CD45+, B220^{lo}, CD3-, intracellular IgG^{hi}) after 6 days of UVR exposure. **(B)** Mice were exposed to a single UVR dose and LCs were sorted from these and control mice 24 hours later. LC expression of EGFR ligands normalized to that of control Balb/c mice. **(C)** MRL-*Fas*^{lpr} LC ADAM17 activity. LCs sorted from MRL-*Fas*^{lpr} mice were treated with PMA or UVR and the percent change in TNFR1 MFI relative to that of untreated LCs was measured 45 minutes later by flow cytometry (n= 6 mice). Dashed lines indicate the relative change in TNFR1 MFI observed in WT mice treated with PMA (green) or UVR (blue) as in Fig. 5A. **(D)** Conditioned supernatants from untreated and UVR-exposed MRL-*Fas*^{lpr} LCs were added to A431 EGFR indicator cells and phosphoEGFR in the A431 cells was measured 10 minutes later by flow cytometry (n= 3 mice). Dashed line indicates the relative change in phosphoEGFR MFI observed with UVR-exposed WT LC supernatants as in Fig. 5C. **(A,B)** Each symbol represents 1 mouse. **(C,D)** Each symbol represents a biological replicate, which is the average of 1-4 replicate wells. Data from 3 **(A,D),** 2 **(B),** and 6 **(C)** independent experiments. Bars represent means and error bars depict standard deviations. n.s.= not significant $p \geq 0.05$, *****$p<0.05$, **$p<0.01$, ***$p<0.001$ using two-tailed unpaired Student's t-test after one-way ANOVA.

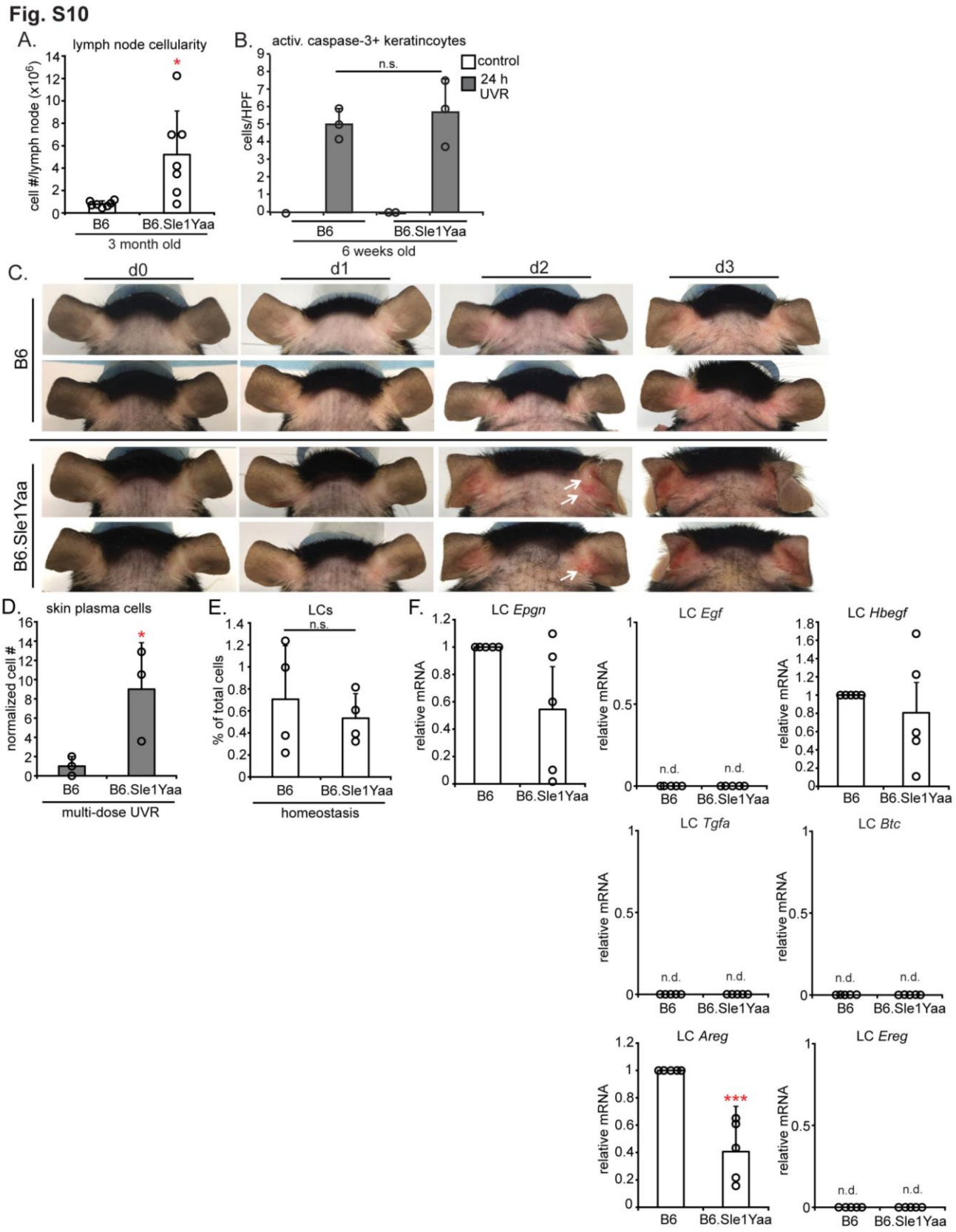

Fig. S10. B6.Sle1yaa mice exhibit photosensitivity and characterization of EGFR ligand expression by their LCs. (A) Popliteal lymph node cellularity at 3 months of age (n= 7 mice).

(B) Activated caspase-3+ keratinocyte numbers in 6 week old B6.Sle1yaa mice or age-matched B6 mice (n= 2-3 mice). **(C,D)** 8-12 month old B6.Sle1yaa mice and age-matched B6 mice were exposed to UVR for 6 days starting at day 0 (d0) and ears harvested 24 hours after the final exposure (n= 3 mice). **(C)** Images of representative ears at the indicated time points of UVR exposure. White arrows indicate visible lesions. **(D)** Normalized number of plasma cells in the skin as measured by flow cytometry. **(E,F)** 8-12 month old B6.Sle1yaa mice or age-matched B6 mice were examined at homeostasis. **(E)** Percent of LCs in skin as measured by flow cytometry (n= 4 mice). **(F)** B6.Sle1yaa LC expression of EGFR ligands. LCs were sorted from homeostatic B6 and B6.Sle1yaa mice and mRNA expression was normalized to that of B6 mice (n= 5 mice). n.d.= not detectable. **(A,B,D-F)** Each symbol represents 1 mouse**.** Data from 7 **(A)**, 3 **(B)**, 2 **(C,D)**, 4 **(E)**, and 5 **(F)** independent experiments. Bars represent means; error bars depict standard deviations. n.s.= not significant $p \geq 0.05$, ***** $p < 0.05$, *** $p < 0.001$ using two-tailed unpaired Student's t-test. T-test was performed after one-way ANOVA for **(B)**.

Fig. S11

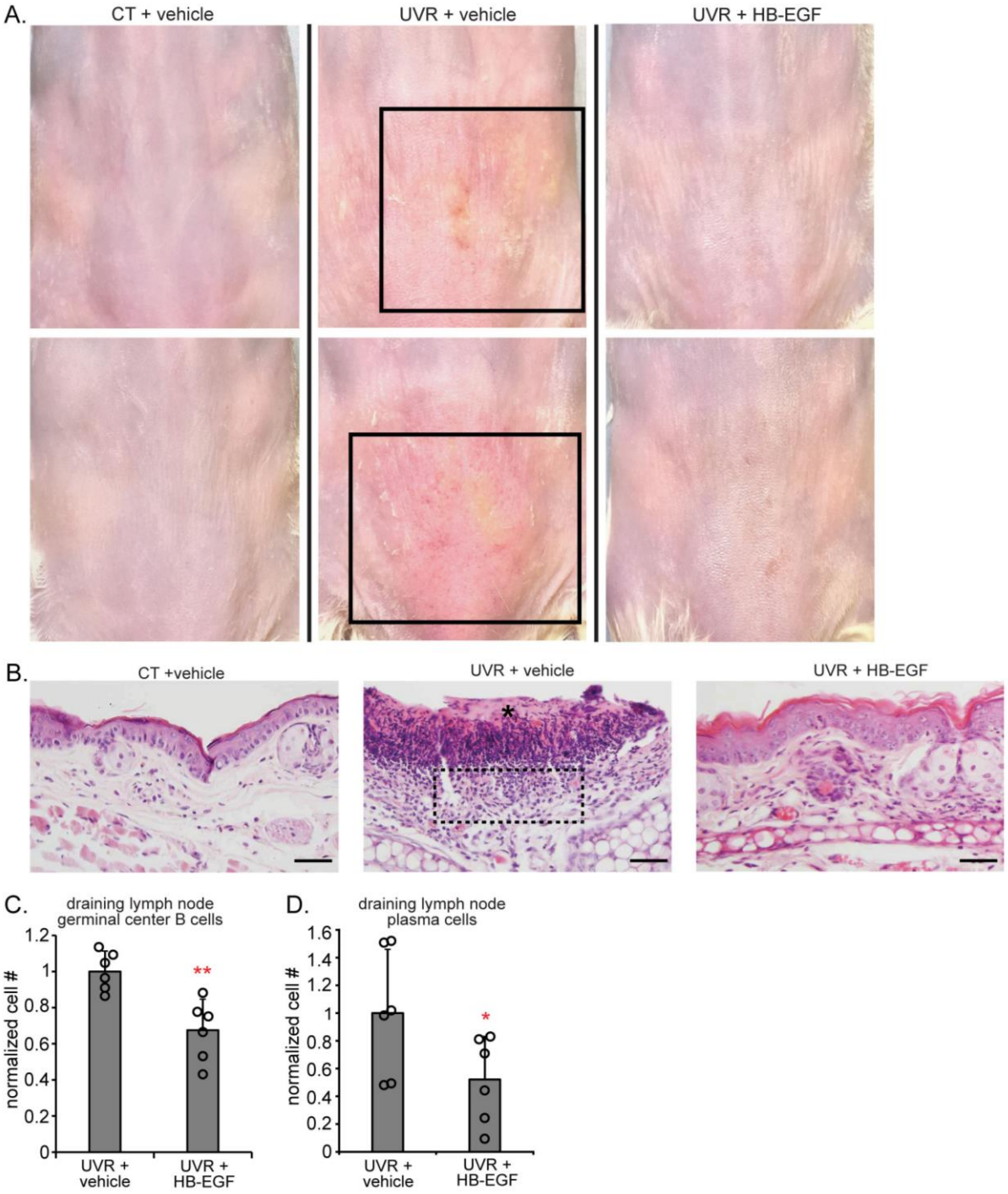

Fig. S11. EGFR ligand application reduces the severity of UVR-induced skin lesions and lymph node B cell responses in SLE model mice. (A-C) Mice were treated with HB-EGF as in Fig. 8A-E (n= 4 mice). **(A)** Magnified images of back lesions as shown in Fig. 8C. Boxes

outline lesional areas. **(B)** Representative H&E images of ear skin. Neutrophil-dominant infiltrate (dashed box); ulceration (*). Scale bar: 50 μm. **(C,D)** Germinal center B cell **(C)** and plasma cell **(D) numbers** in skin draining lymph nodes (auricular and inguinal) normalized to mice treated with UVR+vehicle. **(C,D)** Each symbol represents either inguinal or auricular lymph nodes from multiple mice. Data from 3 **(A,B)** and 2 **(C,D)** independent experiments. Bars represent means. Error bars depict standard deviations. *****$p<0.05$ and **$p<0.01$ using two-tailed unpaired Student's t-test.

Fig. S12

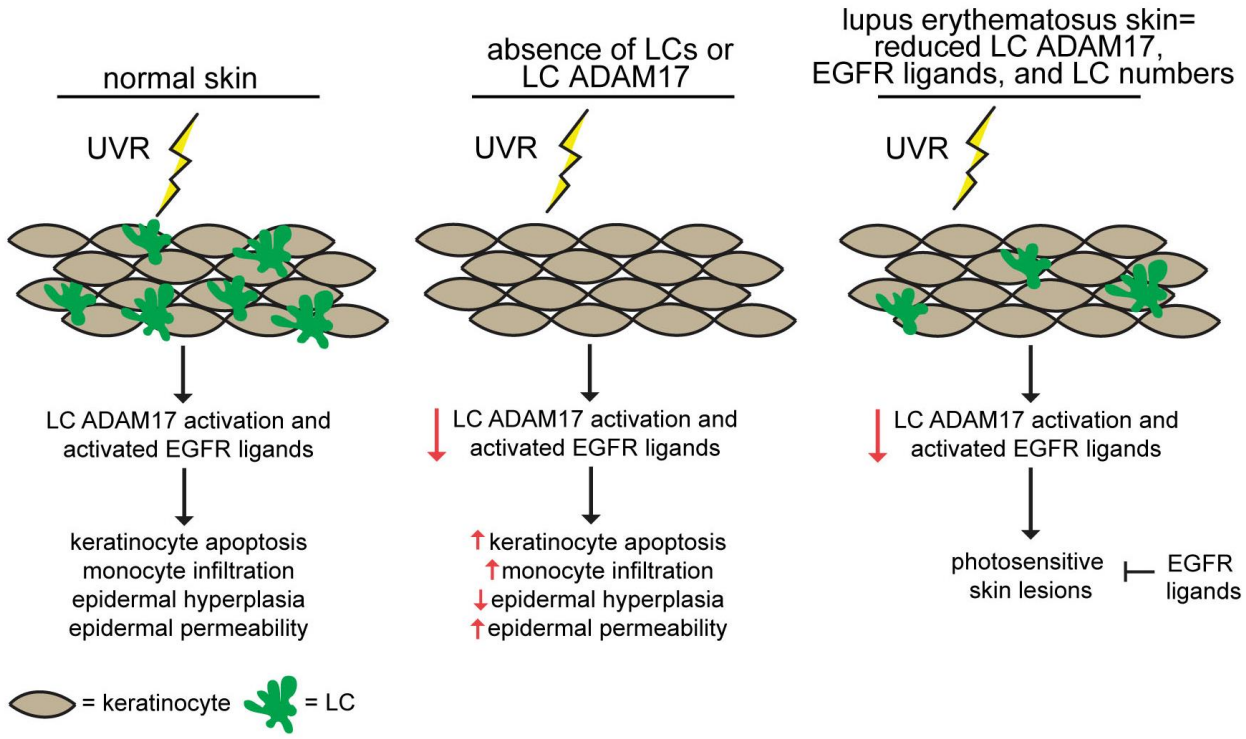

Fig S12. Model of protective LC-keratinocyte axis and dysfunction of this axis in lupus photosensitivity. In normal skin, LCs express ADAM17 and EGFR ligands. UVR stimulates LC ADAM17 activity and LCs provide activated EGFR ligands and limit the extent of keratinocyte apoptosis and skin injury. In the absence of LCs or with ADAM17 deletion in LCs, UVR-induced keratinocyte apoptosis and skin injury are increased. In lupus erythematosus, LCs are less able to provide activated EGFR ligands to keratinocytes, because of reduced ADAM17, reduced EGFR ligand expression, and/or reduced LCs, leading to photosensitivity. The provision of EGFR ligands could be a useful therapeutic approach for photosensitivity.

Fig. S13

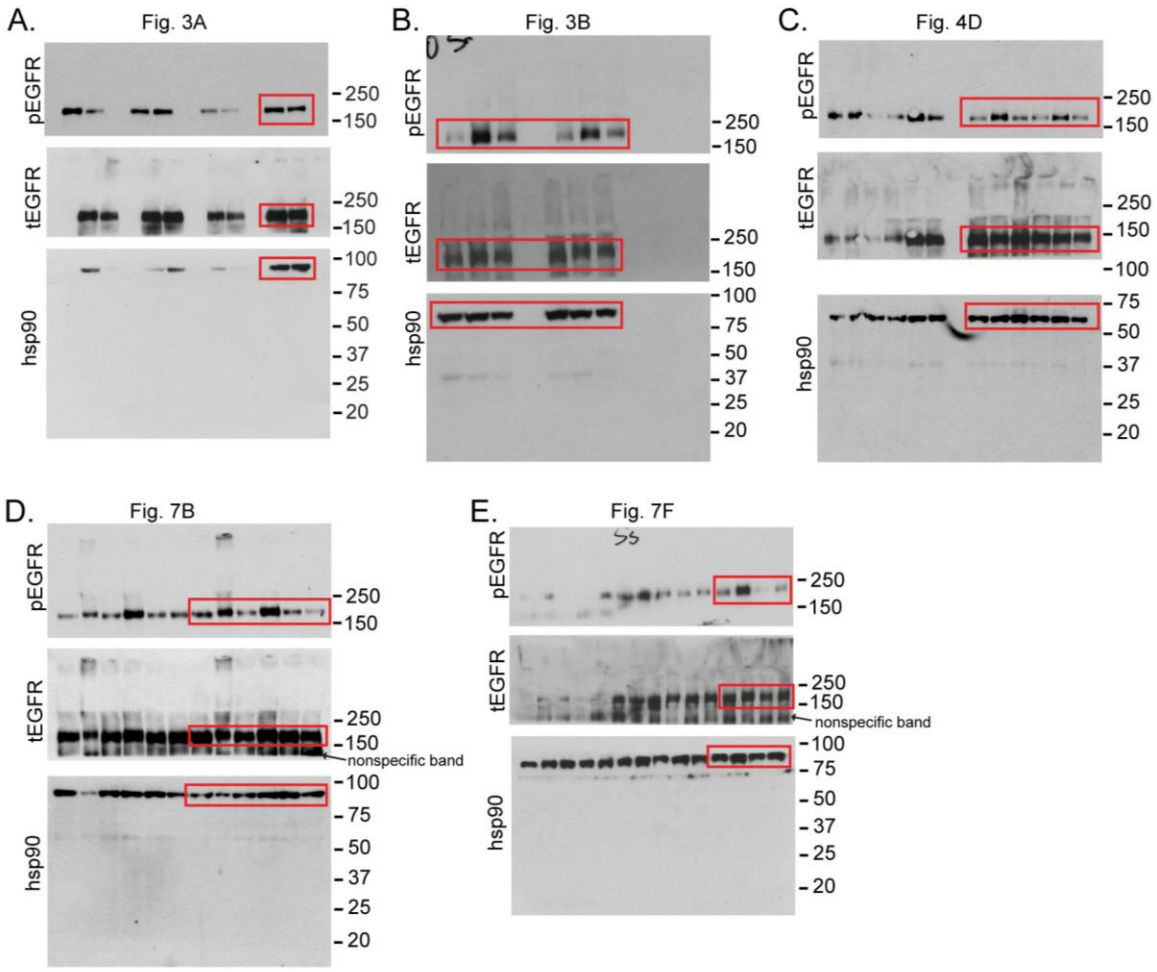

Fig. S13. Uncropped Western blot images. Uncropped Western blot from Fig. 3A **(A)**, Fig. 3B **(B)**, Fig. 4D **(C)**, Fig. 7B **(D)**, and Fig. 7F **(E)**. Western blots were stained with anti-phosphoEGFR (175 kDa) and anti-hsp90 (90 kDa), then stripped and stained with anti-total EGFR (175 kDa). Red boxes indicate the portion of the blots that are included in the main figure and arrows indicate non-specific bands.

Antibody (Clone)	Supplier	Catalog #	Lot #	Used for	Validation
Armenian hamster anti-mouse CD3 biotin (145-2C11)	BioLegend	100304	B216147	FC,IF	By manufacturer
rat anti-mouse Ly6G biotin (1A8)	BioLegend	127604	B218529	FC	By manufacturer
rat anti-mouse B220 biotin (RA3-6B2)	BioLegend	103204	B191786	FC	By manufacturer
rat anti-mouse CD49b biotin (DX5)	eBiosciences	13-5971-81	4295252	FC	By manufacturer
rat anti-mouse CD45 AlexaFlour700 (30-F11)	BioLegend	103128	B211311	FC	By manufacturer
rat anti-mouse CD45 PerCPCy5.5 (30-F11)	BioLegend	103132	B218549	FC	By manufacturer
Armenian hamster CD11c APCCy7 (N418)	BioLegend	117324	B237079	FC	By manufacturer
mouse anti-mouse Iab PE (AF6-120.1)	BioLegend	116408	B177711	FC	By manufacturer
mouse anti-mouse Iab FITC (AF6-120.1)	BDBiosciences	553551	62094	FC	By manufacturer
rat anti-mouse CD24 PerCPCy5.5	BioLegend	101824	B195555	FC	By manufacturer
rat anti-mouse CD11b Brillant Violet 570 (M1/70)	BioLegend	101233	B236974	FC	By manufacturer
rat anti-mouse CD11b PE (M1/70)	BioLegend	101208	B228654	FC	By manufacturer
rat anti-mouse CD11b FITC (M1/70)	BioLegend	101206	B192968	FC	By manufacturer
rat anti-mouse CD3 APCCy7 (145-2C11)	BioLegend	100330	B190252	FC	By manufacturer
rat anti-mouse CD3 FITC (145-2C11)	BDBiosciences	553062	5166876	FC	By manufacturer
rat anti-mouse Ly6C PECy7 (HK1.4)	BioLegend	128018	B242951	FC	By manufacturer
rat anti-mouse Ly6C FITC (HK1.4)	BioLegend	128006	B180475	FC	By manufacturer
mouse anti-mouse CD64 APC (X54-5/7.1)	BioLegend	139306	B207411	FC	By manufacturer
mouse anti-mouse CD64 PE (X54-5/7.1)	BioLegend	139304	B171679	FC	By manufacturer
rat anti-mouse CD31 PerCPCy5.5 (390)	BioLegend	102420	B219868	FC	By manufacturer
rat anti-mouse EpCAM PECy7 (G8.8)	BioLegend	118216	B176413	FC	By manufacturer
rat anti-mouse EpCAM APC (G8.8)	BioLegend	118214	B173069	FC	By manufacturer
rat anti-mouse Sca-1 APCCy7 (D7)	BioLegend	108126	B214144	FC	By manufacturer

rat anti-mouse CD49f biotin (GoH3)	BioLegend	313604	B226568	FC	By manufacturer
Armenian hamster anti-mouse CD103 PE (2E7)	BioLegend	121406	B184715	FC	By manufacturer
Armenian hamster anti-mouse CD103 APC (2E7)	BioLegend	121413	B222546	FC	By manufacturer
Armenian hamster TNFR1/p55 APC (55R-286)	BioLegend	113005	B240777	FC	By manufacturer
rat anti-mouse IgG1 FITC (A85-1)	BDBiosciences	553443	92966	FC	By manufacturer
rat anti-mouse IgG2a/2b FITC (R240)	BDBiosciences	553399	4150540	FC	By manufacturer
rat anti-mouse IgG3 FITC (R40-82)	BDBiosciences	553403	7027876	FC	By manufacturer
rat anti-mouse CD138 APC (281-2)	BioLegend	142505	B237677	FC	By manufacturer
peanut agglutinin (PNA) biotin	Vector Labs	B-1075	X1221	FC	By manufacturer
mouse anti-human CD1a AlexaFlour 647 (HI149)	BioLegend	30016	B236344	FC	By manufacturer
mouse anti-human HLA-DR (L243)	BioLegend	307606	B183424	FC	By manufacturer
mouse anti-human CD45 PerCPCy5.5 (HI30)	eBiosciences	45-0459-71	E029129	FC	By manufacturer
goat anti-mouse,human Langerin (E-17)	Santa Cruz Biotechnology	sc-22620	D2216	IF	By manufacturer
rabbit anti-mouse,human active caspase-3 (polyclonal)	R&D Systems	AF835	CF23415101	IF	By manufacturer
rabbit anti-human phospho-EGFR Tyr1068 (EP774Y)	BioCare Med.	API300AA	013117	IF	By manufacturer
mouse anti-human EGFR (H11)	BioCare Med.	ACI063A	060517	IF	By manufacturer
rabbit anti-mouse phospho-EGFR Tyr1068 (D7A5)	Cell Signaling	3777S	13	FC, WB	By manufacturer and Fig. S4A,B
goat anti-mouse total EGFR (polyclonal)	R&D Systems	AF1280	HXO0216012	FC, WB	By manufacturer
rabbit anti-mouse hsp90 (polyclonal)	Cell Signaling	4874S	3	WB	By manufacturer
goat IgG polyclonal isotype control	R&D Systems	AB-108-C	ES4115041	FC,IF	By manufacturer
rat IgG2a isotype control (R35-95)	BDBiosciences	553928	4324804	FC	By manufacturer
rabbit monoclonal IgG isotype control (DA1E)	Cell Signaling	3900S	25	IF	By manufacturer
mouse IgG isotype control (#11711)	R&D	MAB002	1X12070	IF	By

	Systems		41		manufacturer
human monoclonal anti-human IgG1 ADAM17 (D1(A12))	Abcam	215268	GR3192882-1	FB, FC	By manufacturer
monoclonal human IgG1 isotype control	Adipogen	AG-35B-0006-C100	A26741504	FB, FC	By manufacturer
mouse anti-human CD3 PECy7 (UCHT1)	BioLegend	300419	B208514	FC	By manufacturer
mouse anti-human HLA-DR APC-Cy7 (L243)	BioLegend	307617	B246747	FC	By manufacturer
mouse anti-human EpCAM APC (9C4)	BioLegend	324207	B155666	FC	By manufacturer
mouse anti-human CD1a PE (BL6)	Beckman Coulter	IM1942U	11	FC	By manufacturer

Table S1. List of primary antibodies. FC= Flow Cytometry, IF= Immunofluorescence, WB= Western Blot, FB= Functional Blocking

Antibodies (Clone)	Supplier	Catalog Number	Lot Number	Application
donkey anti-goat Alexa Fluor 488 (polyclonal)	Jackson Immunoresearch	705-545-003	128611	FC
donkey anti-rabbit Alexa Fluor 647 (polyclonal)	Jackson Immunoresearch	711-606-152	125599	FC
Streptavidin Pacific Blue	ThermoFisher Scientific (Invitrogen)	S11222	1870540	FC
Streptavidin APC	ThermoFisher Scientific (Invitrogen)	S868	1124091	FC
Streptavidin Alexa Flour 488	ThermoFisher Scientific (Invitrogen)	S11223	1851449	FC, IF
donkey anti-mouse IgG biotin	Jackson Immunoresearch	715-066-151	124850	IF
donkey anti-human IgG biotin	Jackson Immunoresearch	709-066-098	135590	FC
donkey anti-rabbit rhodamine	Jackson Immunoresearch	711-295-152	130068	IF
donkey anti-goat Alexa Flour 647	Jackson Immunoresearch	705-605-147	124186	IF
donkey anti-rabbit HRP	Jackson Immunoresearch	711-035-152	128838	WB
donkey anti-goat HRP	Jackson Immunoresearch	705-035-003	130633	WB
Human TruStain FcX (Fc Receptor Blocking Solution)	BioLegend	422301	B247180	FC
DAPI	ThermoFisher Scientific (Invitrogen)	D1306	1023584	FC,IF

Table S2: Secondary antibodies and other staining reagents. FC= Flow Cytometry, IF= Immunofluorescence, WB= Western Blot